Integrated Multi-Mission Ocean Altimeter Data for Climate Research TOPEX/Poseidon, Jason-1, 2, & 3
User's Handbook
Version 5.0

Copyright 2020 California Institute of Technology.
All rights reserved.

Table of Contents

INTRODUCTION **1**

1.0 GENERAL STRUCTURE CHARACTERISTICS **1**
1.1 GEO-REFERENCED 1HZ SSH 2
1.2 CONSTRUCTION OF THE CORRECTED SSH ANOMALY 3
1.3 SSH QUALITY FLAG WORD 7

2.0 VERSION 5.0 REVISIONS TO SSH COMPUTATION **9**
2.1 THE GSFC REPLACEMENT ORBIT HEIGHT CORRECTION 9
2.2 RE-CALIBRATED JASON-1 MICROWAVE RADIOMETER JMR) 14
2.3 TOPEX MICROWAVE RADIOMETER (TMR) ENHANCED WET PATH DELAYS 16
2.4 OCEAN TIDE CORRECTIONS 17
2.5 POLE TIDE CORRECTION 18
2.6 MEAN SEA SURFACE 19

3.0 INTER-MISSION BIASES **20**
3.1 SEA STATE BIAS 20
3.2 JASON-1, 2, & 3 VERIFICATION PHASE RESULTS 21
3.3 TIDE GAUGE VALIDATIONS 23

4.0 ESTIMATION OF GLOBAL AND REGIONAL MEAN SEA LEVEL **26**

5.0 REFERENCES **29**

APPENDIX I: QUALITY FLAG BIT DISTRIBUTIONS **33**

APPENDIX II: SEA STATE BIAS SPECIFICATIONS **41**

Table of Figures

FIGURE 1: GDR CONVENTION **2**

FIGURE 2: 1HZ SSH CONSTRUCTED AT REFERENCE ORBIT LOCATIONS IS ACHIEVED BY RE-SAMPLING HIGH-RATE SSH FROM CONTIGUOUS 1HZ GDR SSH EVALUATED AT MID-POINT ... **3**

FIGURE 3: COASTAL BITS **8**

FIGURE 4A. STD2006 RADIAL ORBIT ACCURACY RELATIVE TO DPOD2014 USING INDEPENDENT CROSSOVER DATA **14**

FIGURE 4B. MEAN RADIAL STD2006-DPOD2014 ORBIT DIFFERENCES/CYCLE OVER WATER **15**

FIGURE 5A: JMR (GDR_C) MINUS ECMWF MEAN PATH DELAY DIFFERENCES DETECT TIMES WHERE FURTHER RE-CALIBRATION IS WARRANTED. **15**

FIGURE 5B: RE-CALIBRATED JMR VERSUS MERRA AND ECMWF MODEL WET PATH DELAYS SUGGEST JMR DRIFT RATE LESS THAN 1MM/DECADE. **17**

FIGURE 6: ENHANCED GDR_E JMR PATH DELAYS RECOVERED NEAR LAND VIA MIXED PIXEL (MP) ALGORITHMS PROVIDE IMPROVED ACCURACIES IN COASTAL AREAS. **18**

FIGURE 7: THE MP ALGORITHM SUCCESSFULLY COMPENSATES FOR LAND CONTAMINATION. 19

FIGURE 8: THE RESULTANT AMPLITUDE OF THE 59-DAY SIGNAL THAT VARIES IN T/P, JASON-1, AND JASON-2 GMSL ESTIMATES WITH THE APPLICATION OF OCEAN TIDE MODEL, AND THE APPLICATION OF CG TO T/P ALTIMETRY. 20

FIGURE 9: REGIONAL LINEAR TRENDS OF POLE TIDE DIFFERENCES 21

FIGURE 10: CROSS-TRACK SLOPES EVALUATED AT GEO-REFERENCED LOCATIONS OVER OCEAN BASED ON DTU15 MSS. 22

FIGURE 11: MEAN DIFFERENCES OF SSH BETWEEN HEIGHTS BASED ON PARAMETRIC VERSUS NON-PARAMETRIC SEA STATE BIAS SOLUTIONS REVEALS SEPARATE BIASES FOR TOPEX SIDE A AND FOR SIDE B 23

FIGURE 12: JASON-1 MINUS TOPEX INTER-MISSION BIAS IS ESTIMATED FROM AVERAGED SSH COLLINEAR RESIDUALS DURING THE JASON-1 VERIFICATION PHASE 24

FIGURE 13: JASON-2 MINUS JASON-1 INTER-MISSION BIAS IS ESTIMATED FROM AVERAGED SSH COLLINEAR RESIDUALS DURING JASON-2 VERIFICATION PHASE 25

FIGURE 14: JASON-3 MINUS JASON-2 INTER-MISSION BIAS IS ESTIMATED FROM AVERAGED SSH COLLINEAR RESIDUALS DURING JASON-3 VERIFICATION PHASE 25

FIGURE 15: CURRENT NETWORK OF 64-TIDE GAUGE SITES 26

FIGURE 16: ESTIMATE OF TOPEX SIDE A/B BIAS IS DERIVED FROM PER CYCLE MEAN COMPARISONS OF ALTIMETER SSH VARIATIONS WITH HEIGHT VARIATIONS FROM 64-SITE TIDE GAUGE NETWORK 27

FIGURE 17: POSEIDON-1 BIAS WITH RESPECT TO TOPEX IS ESTIMATED VIA MEAN COLLINEAR T/P SSH RESIDUALS 28

FIGURE 18: RESULTANT PER CYCLE COMPARISONS OF ALTIMETER DERIVED SSH VARIATIONS WITH HEIGHT VARIATIONS FROM 64-SITE TIDE GAUGE NETWORK AFTER APPLICATION OF INTER-MISSION BIASES TO FORM A SINGLE ADJUSTED SSH CLIMATE DATA RECORD 28

FIGURE 19: GLOBAL MEAN SEA LEVEL IS ESTIMATED AT 3.3 ± 0.4 MM/YR (GIA APPLIED) BASED ON SSH VARIATIONS WITH RESPECT TO 20-YEAR TOPEX/JASON MEAN PROFILE 29

FIGURE 20: GLOBAL MEAN SEA LEVEL VARIATIONS WITH ANNUAL AND SEMI-ANNUAL SIGNALS REMOVED. 30

FIGURE 21: REGIONAL MEAN SEA LEVEL VARIATIONS ESTIMATED AT EACH GEO-REFERENCED LOCATION 30

FIGURE A-1: QUALITY FLAG WORD BIT #1 33

FIGURE A-2: QUALITY FLAG WORD BIT #2 33

FIGURE A-3: QUALITY FLAG WORD BIT #3 34

FIGURE A-4: QUALITY FLAG WORD BIT #4 34

FIGURE A-5: QUALITY FLAG WORD BIT #5 35

FIGURE A-6: QUALITY FLAG WORD BIT #6 35

FIGURE A-7: QUALITY FLAG WORD BIT #7 36

FIGURE A-8: QUALITY FLAG WORD BIT #8 ..... **36**
FIGURE A-9: QUALITY FLAG WORD BIT #9 ..... **37**
FIGURE A-10: QUALITY FLAG WORD BIT #10 ..... **37**
FIGURE A-11: QUALITY FLAG WORD BIT #11 ..... **38**
FIGURE A-12: QUALITY FLAG WORD BIT #12 ..... **38**
FIGURE A-13: QUALITY FLAG WORD BIT #13 ..... **39**
FIGURE A-14: QUALITY FLAG WORD BIT #14 ..... **39**
FIGURE A-15: QUALITY FLAG WORD BIT #15 ..... **40**
FIGURE A-16: ALL QUALITY FLAG WORD BITS **40**
FIGURE A-17: QUALITY FLAG WORD COASTAL BITS **41**

Brian Beckley	KBR, Inc.
Richard Ray	NASA/GSFC
Nikita Zelensky	University of Maryland
Frank Lemoine	NASA/GSFC
Xu Yang	KBR Inc.
Shannon Brown	JPL/Caltech/NASA
Shailen Desai	JPL/Caltech/NASA
Gary Mitchum	University of South Florida

Introduction

Maintenance and improvements to the fidelity of the TOPEX/Poseidon, Jason-1, Jason-2/OSTM, and Jason-3 (TPJAOS) Sea Surface Height Climate Data Record (SSH CDR) is a continuous effort through the research activities of the Ocean Surface Topography Science Team (OSTST). As further advancements and/or re-calibrations are made to any of the correction parameters or models, the TPJAOS product is recalculated with the most accurate algorithms sanctioned by the OSTST. Notification and details of revisions to the TPJAOS will be provided and announced by the Physical Oceanography Distributed Active Archive Center (PODAAC) and displayed at this site http://podaac.jpl.nasa.gov/Integrated_Multi-Mission_Ocean_AltimeterData. Users will be notified of revisions to ensure they are consistently up to date.

A number of algorithm revision/improvements along with the integration of Jason-3 data prompted the release of a revised version 4.0 in March of 2017. In summary the following revisions were incorporated in the development of TPJAOS version 4.0:

- GSFC itrf2014/dpod4-based orbit replacing std1504 for all missions
- Extending SSH time series with Jason-3 altimetry
- DTU15 MSS reference
- Cross-track gradient correction based on DTU15 MSS derived cross-track slopes
- Revised inter-mission bias estimates

A minor revision (v4.1) was implemented to reprocess the orbits for a few Jason-3 cycles with improved DORIS tracking. The most recent update (version 4.2) involved the removal of the TOPEX cal-1 mode range correction (Beckley et al., 2017) and the subsequent inter-mission bias revisions. The following sections of this report detail these previous and current v5.0 revisions to the SSH record, and any subsequent impacts to validation results and mean sea level estimates. Users are referred to the Version 1.0 and 2.0 handbooks (ftp://podaac.jpl.nasa.gov/allData/merged_alt/preview/L2/docs/) for algorithm specifications that have remained unchanged.

1.0 General Structure Characteristics

The MEaSURE's TPJAOS v5.0 sea surface height (SSH) anomaly product is a multi-mission data set comprised of TOPEX/Poseidon (T/P), Jason-1, OSTM (Jason-2), and Jason-3 altimeter data integrated to form a single SSH Climate Data Record (CDR). Altimeter data from the multi-mission Geophysical Data Records (GDRs) are interpolated to a common reference orbit facilitating direct time series analysis of the geo-referenced SSH. The baseline v5.0 merged file is comprised of 1,020 (updated September 2020 from 989) 10-day repeat cycles:

Cycle	1 – 355	T/P (cycles 1 – 355)
	356 – 582	Jason-1 (cycles 13 -239)
	583 – 865	Jason-2 (cycles 1 – 283)
	866 – 1,020	Jason-3 (cycles 4 - 158)

As future Jason-3 cycles become available the direct access structure of the file allows new data to be appended. All inter-mission biases have been applied to provide a seamless transition throughout the current 27+ year record.

Each 10-day repeat cycle is comprised of 127 revolutions. Each revolution has 6745 along-track locations spanning the equatorial ascending node (Figure 1).

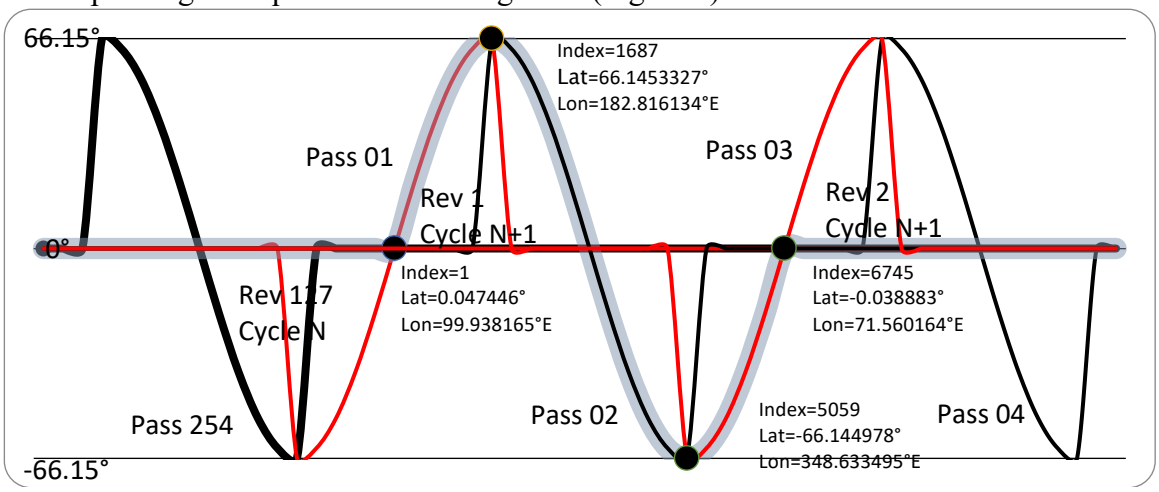

Figure 1 : GDR convention of ascending odd numbered passes (solid red lines) and descending even numbered passes (solid black lines) total 254 passes/repeat cycle. The MEaSURE's product convention is based on 127-revolutions/repeat cycle. Revolution #1 is shown (blue shading overlay) with reference orbit lat/lon coordinates indicated for first and last geo-reference index, and for index at maximum and minimum latitude.

Each SSH data record is a SSH time series at a specific geo-referenced location defined by revolution number and along-track index. A 3-dimensional directory (rev#, index, cycle) permits direct access of individual locations at specific times (i.e. temporal and spatial sub-sampling). Auxiliary files provide time, mean sea surface reference, terrain type, bathymetry, proximity to coast, and SSH quality assessments (flag word) at each geo-referenced location.

1.1 Geo-referenced 1Hz SSH

Construction of the 1Hz geo-referenced SSH is achieved by sampling the GDR high-rate SSH (10Hz for T/P and 20Hz for Jason-1 and OSTM) from contiguous 1Hz samples that align with the reference index location, and the time at the reference location derived from the GDR (Figure 2).

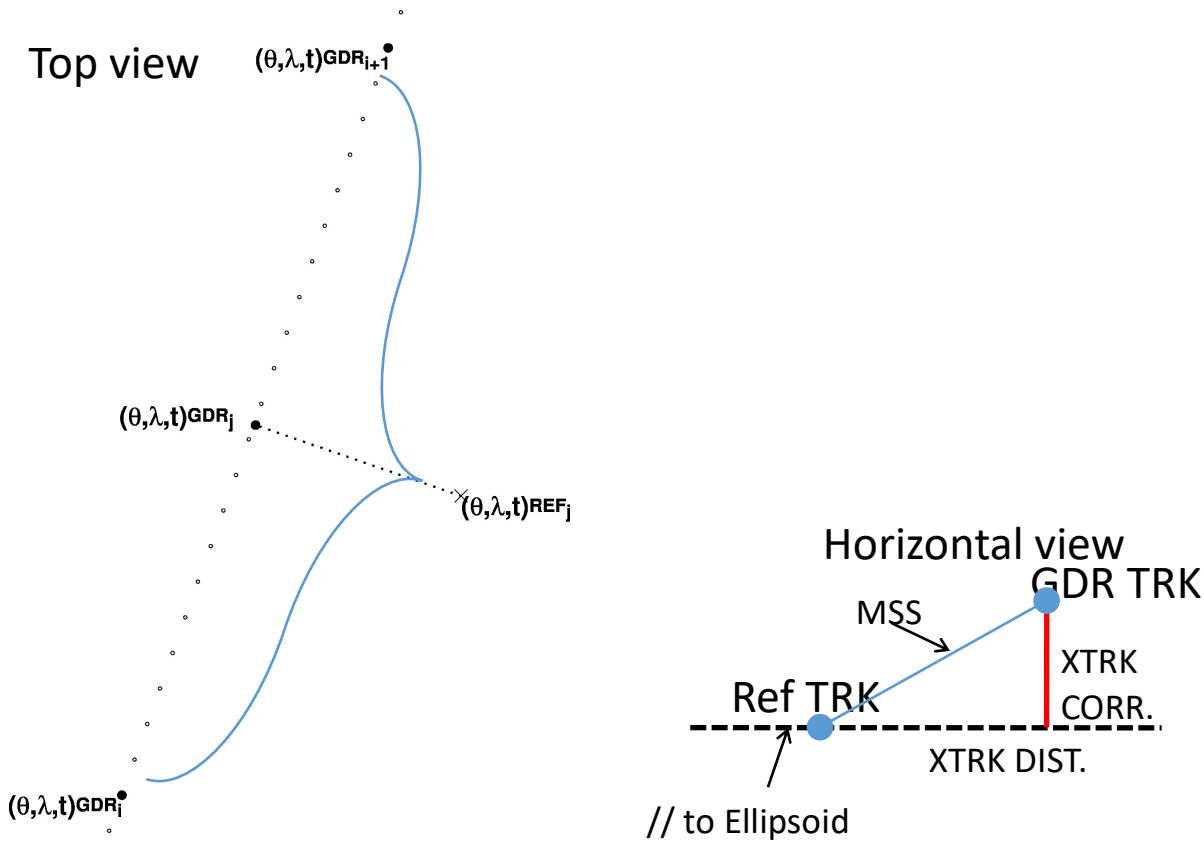

Figure 2: 1Hz SSH constructed at reference orbit locations (REF $_j$) is achieved by re-sampling high-rate SSH from contiguous 1Hz GDR SSH (GDR $_i$ and GDR $_{i+1}$) evaluated at mid-point GDR $_j$.

Satellites can deviate from the nominal orbit ground track by up to ± 1 km. To correct for this, a Mean Sea Surface [MSS] model can be used to effect a cross-track transformation between the along-track SSH and the corresponding SSH on the reference orbit. Towards this end, the normal projected onto the GDR groundtrack from the reference location provides the cross-track distance. The product of the cross-track distance and the local slope of the DTU15 MSS (Andersen et al., 2015) provide the cross-track gradient correction (Brenner et al, 1990) applied to account for local MSS gradients. The regression fit of the high-rate SSH is performed employing the GDR routine g1071 (TOPEX Ground System Science Algorithm Specification, 1991). Additional constraints require a minimum number of high-rate SSH (6 for T/P, and 16 for Jason-1, 2 and 3), and a minimum number of high-rate SSH on each side of the midpoint (2 for T/P and 7 for Jason-1, 2, and 3). The standard deviation of the high-rate residuals with respect to the resultant 1Hz average fit is computed and incorporated in the SSH quality assessment flag word (see Table 2).

1.2 Construction of the Corrected SSH Anomaly

SSH $_{uncorrected}$ = Orbit (GSFC itrf2014/std2006) – Range_ku $_{corrected\ (net_instrument_corection_ku)}$
SSH $_{corrected}$ = SSH $_{uncorrected}$ - Dry Troposphere Delay

- Wet Troposphere Delay
- Solid Earth Tide
- Ocean Tide
- Ocean Load Tide
- Long-Period Tide
- Internal Tide
- Pole Tide
- Ionosphere Delay
- Sea State Bias (SSB) Delay
- Atmospheric Load (IB)
- Cross-track gradient
+ inter-mission bias

$SSH_{anomaly} = SSH_{corrected}$ - DTU15 mean sea surface

Note: The SSH anomalies are with respect to DTU15 MSS. The user can construct SSH anomalies with respect to a collinear mean reference by first adding back the DTU15 MSS, which is made available as a separate auxiliary file.

The GDR heritage for each mission:

- T/P MGDR_B (Benada, 1997)
- Jason-1 GDR_E (Picot et al., 2016)
- OSTM GDR_D (OSTM/Jason-2 products handbook, December 2011)
- Jason-3 GDR_D (Jason-3 Products handbook, February 2016)

Origination of individual range and geophysical corrections applied to the SSH for each mission is detailed in table 1. Corrections employed that were directly obtained from GDR are identified by their parameter name as in handbook in bold italics. Many of the altimeter corrections present on the mission GDRs have been recomputed to take advantage of more recent and accurate models and to insure consistency across missions. The development and implementation of replacement or revised correction parameters are explained in sections below.

Table 1: Heritage of range and geophysical corrections applied to the SSH for each mission.

	TOPEX	Poseidon-1	Jason-1	Jason-2 (OSTM)	Jason-3
Orbit	GSFC std2006 referenced to ITRF2014 (Altamimi et al., 2016)	GSFC std2006 referenced to ITRF2014 (Altamimi et al., 2016)	GSFC std2006 referenced to ITRF2014 (Altamimi et al., 2016)	GSFC std2006 referenced to ITRF2014 (Altamimi et al., 2016)	GSFC std2006 referenced to ITRF2014 (Altamimi et al., 2016)
Range Ku	***Net_Instr_R_Corr_K*** Cal-1 mode & Cg *range correction NOT applied (Beckley et al. , 2017)*	***Net_Instr_R_Corr_K*** Cg *range correction NOT applied*	***net_instr_corr_range_ku***	***net_instr_corr_range_ku***	***net_instr_corr_range_ku***

Dry Trop.	ECMWF Interim Re-analysis	ECMWF Interim Re-analysis	ECMWF operational ***model_dry_tropo_corr***	ECMWF operational ***model_dry_tropo_corr***	ECMWF operational ***model_dry_tropo_corr***
Wet Trop.	TMR enhanced replacement product (2015)	TMR enhanced replacement product (2015)	GDR_E JMR ***rad_wet_tropo_corr***	GDR_D AMR ***rad_wet_tropo_corr***	GDR_T AMR ***rad_wet_tropo_ corr***
Ocean Tide	GOT4.8	GOT4.8	GOT4.10	GOT4.10	GOT4.10
Ocean Load Tide	GOT4.8	GOT4.8	GOT4.10	GOT4.10	GOT4.10
Long-Period Tide	Ray & Erofeeva (2014)	Ray & Erofeeva (2014)	Ray & Erofeeva (2014)	Ray & Erofeeva (2014)	Ray & Erofeeva (2014)
Internal Tide	Ray & Zaron (2016)	Ray & Zaron (2016)	Ray & Zaron (2016)	Ray & Zaron (2016)	Ray & Zaron (2016)
Pole Tide	Desai et al., 2015	Desai et al., 2015	Desai et al., 2015	Desai et al., 2015	Desai et al., 2015
Solid Earth Tide	***H_Set***	***H_Set***	***solid_earth_tide***	***solid_earth_tide***	***solid_earth_tide***
Iono	Dual-frequency ***Iono_Corr (smoothed)***	Doris/GIM ***Iono_Dor***	Dual-frequency ***iono_corr_alt_ku (smoothed***	Dual-frequency ***iono_corr_alt_ku (smoothed)***	Dual-frequency ***iono_corr_alt_ku (smoothed)***
Sea State Bias	Non-parametric collinear residuals (Tran, et. al , 2010)	Parametric BM4 crossover residuals (Gaspar et al 1994) ***EMB_Gaspar***	Non-parametric collinear residuals (Tran et. al, 2012) ***sea_state_bias_ku***	Non-parametric collinear residuals (Tran et al 2013)	Non-parametric collinear residuals (Tran et al 2016)
Atmos-pheric load	Dynamic Atmospheric Correction (DAC)	Dynamic Atmospheric Correction (DAC)	ECMWF operational + MOG2D hi-frequency ***inv_bar_corr + hf_fluctuations corr***	ECMWF operational + MOG2D hi-frequency ***inv_bar_corr + hf_fluctuations corr***	ECMWF operational + MOG2D hi-frequency ***inv_bar_corr + hf_fluctuations corr***
Cross-Track gradient	DTU15 MSS	DTU15 MSS	DTU15 MSS	DTU15 MSS	DTU15 MSS

Inter-mission range bias	23.9 + 0.2 mm (AltB wrt J1/J2 level) -6.7 mm (AltA wrt adjusted AltB)	26.1 mm wrt J1/J2 level (< cycle 132) 20.2 mm wrt adjusted TOPEX (> cycle 132)	0.2 mm wrt Jason-2	0.0 mm	29.0 mm wrt Jason-2

A SSH anomaly with respect to the DTU15 mean sea surface (Andersen, 2016) is computed if all correction fields are available (i.e. various conventions used throughout not set to default value). If one or more of the corrections applied are outside accepted nominal ranges, a quality assessment flag word bit is set to indicate the less than optimal quality. This rationale allows maximum retention of coastal and inland water observations that may otherwise be edited as "blunders" by open ocean standards. Table 2 lists the nominal ranges for each correction that with few exceptions follows the GDR handbook recommendations.

Table 2: Nominal ranges for individual correction parameters. Quality flag word bit #6 (see SSH Quality Flag Word description below) is set if any single correction parameter is outside nominal range.

Correction parameter	Nominal range
Dry Troposphere	> -2600 mm and < -1900 mm
Wet Troposphere	≥ -600 mm and < 0 mm
Ocean Tide	> -5 m and < + 5 m
Load Tide	> -150 mm and < +150 mm
Pole Tide	≥ -100 mm and ≤ +100 mm
Solid Earth Tide	≥ -1000 mm and ≤ +1000 mm
Sea State Bias	≥ -600 mm and ≤ 0 mm
Altimeter derived wind speed	≥ 0 m/s and < 25 m/s
Atmospheric load	≥ -1000 mm and ≤ +1000 mm

1.3 SSH Quality Flag Word

For each 1Hz geo-referenced SSH anomaly, a flag word is assigned to further assess the quality of the resultant SSH determination and provide the capability for tailored edit strategies for particular user applications.

Bit 0 : blank
Bit 1 : = 0 Dual-frequency altimeter measurement
= 1 Single frequency altimeter measurement
Bit 2 : = 0 depth ≥ 200 meters
= 1 depth < 200 meters
Bit 3 : = 0 proximity to land ≥ 50 km
= 1 proximity to land < 50 km
Bit 4 : = 0 Sigma H of fit < 15 cm (< 20 cm for Poseidon-1)
= 1 Sigma H of fit ≥ 15 cm (≥ 20 cm for Poseidon-1)
Bit 5 : = 0 high rate SSH sampled from two contiguous 1Hz data observations
= 1 high rate SSH sampled from single 1Hz observation
Bit 6 : = 0 all SSH corrections within nominal range
= 1 one or more of SSH corrections outside nominal range
Bit 7 : = 0 Cross Track Distance < 1.0 km.
= 1 Cross Track Distance ≥ 1.0 km.
Bit 8 : = 0 Cross Track Slope < 10 cm/km.
= 1 Cross Track Slope ≥ 10 cm/km.
Bit 9 : = 0 Significant Wave Height < 8 m and > 0 m(Ku band)
= 1 Significant Wave Height ≥ 8 m or = 0 m(Ku band)
Bit 10 : = 0 Sea ice not detected
= 1 Sea ice detected
Bit 11 : = 0 No rain contamination detected
= 1 Possible rain contamination detected.
Bit 12 : = 0 Sigma0 ≥ 6 db and ≤ 27 db (Ku band)
= 1 Sigma0 < 6 db or > 27 db (Ku band)
Bit 13 : = 0 Attitude (Att_Wvf) ≥ 0 and ≤ 0.3 degrees (T/P)
= 0 off_nadir_angle_ku_wvf ≥ -.09 deg^2 and ≤ +.09 deg^2
= 1 Attitude (Att_Wvf) < 0 or > 0.3 degrees (T/P)
= 1 off_nadir_angle_ku_wvf < -.09 deg^2 or > +.09 deg^2
Bit 14 : = 0 radiometer observation NOT suspect (tmr_bad set=0)
= 1 radiometer observation suspect (tmr_bad set > 0)
Bit 15 : = 0 GOT4.8 minus FES04 tide models differ by ≤ 2 cm.
= 1 GOT4.8 minus FES-4 tide models differ by > 2 cm.

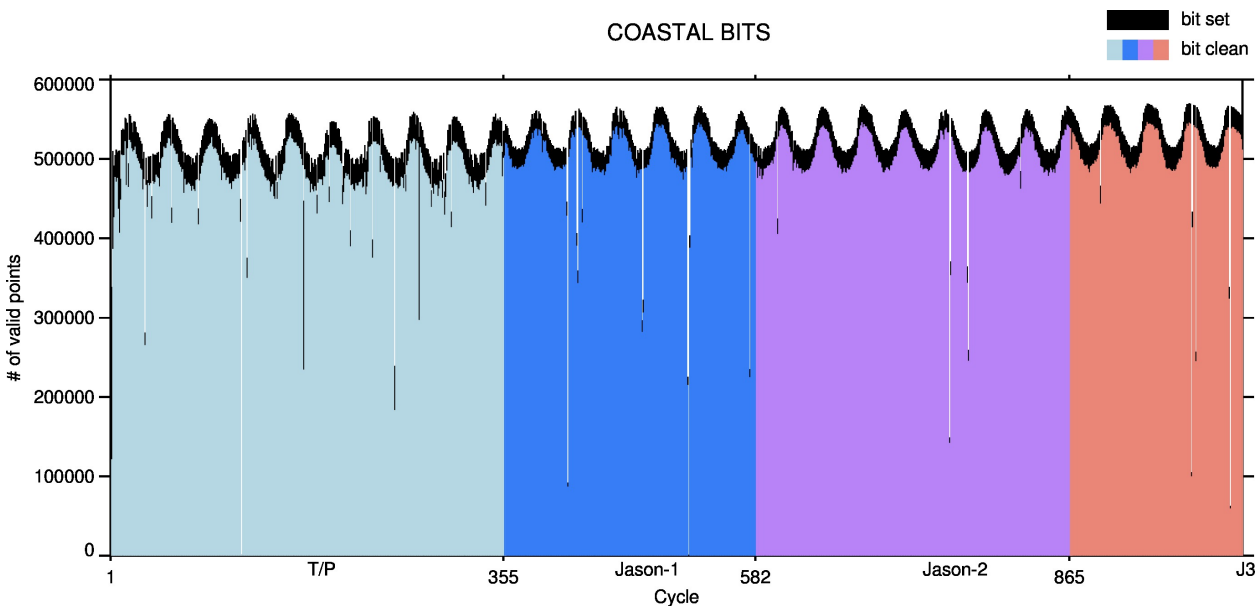

Figure 3: Approximately 5% of valid (not set to default value of 32767) open ocean SSH anomalies are edited based on an edit strategy that requires bits 4-14 pass (i.e. equal 0). Bits 2,3, and 15 are not checked thus retaining coastal observations.

2.0 Version 5.0 and Version 4.2 addendum revisions to SSH computation

2.1 The GSFC replacement orbit height correction

Accurate orbit determination is central to the computation of the altimeter-derived surface elevation observation. The orbit defines the geocentric reference for the satellite altimeter sea surface measurement. Orbit accuracy and consistency are essential not only to the altimeter measurement accuracy across one mission, but also for the seamless transition between missions (Beckley, et. al, 2004). The analysis of altimeter data for TOPEX/Poseidon (TP), Jason-1 (J1), Jason-2 (J2), and Jason-3 (J3) requires that the orbits for all four missions be in a consistent reference frame, and calculated with the best possible standards to minimize error and maximize the data return from the time series, particularly with respect to the demanding application of consistently measuring global sea level change. This multi-mission altimetry time series can provide unprecedented insight into long-period ocean/atmosphere coupling needed for better understanding climate change. There are very demanding 1-cm radial orbit accuracy and cross-mission consistency objectives required to meet this goal (Cazenave et al., 2009, Ablain et al., 2009, Beckley et al., 2010). The orbit is also essential to calibrating the altimeter range, other altimeter corrections such as the sea state bias, and the inter-mission range bias. Such MEaSURE's altimeter bias corrections are based on the same orbits as are used for the geocentric height correction described in this section. Furthermore, altimeter data accuracy must be improved in order to answer today's important questions such as: ''is the global mean sea level rise accelerating? (Fasullo et al., 2016)", ''can regional sea level rates be forecast for better flood planning?", ''can an anthropogenic footprint be seen in the sea level changes? (Palanisamy et al., 2015). Considering the GCOS (GCOS, 2011) analysis, Ablain et al. (2015) have estimated altimeter data accuracy requirements for responding to these and other such questions. The requirements call for accuracies of 0.3 mm/year on a global scale, and to better than 1 mm/year on a regional scale.

Ensuring the highest accuracy and consistency of the satellite orbit is a critical component of the MEaSURE's task. Foremost is the application of improved GSFC replacement orbits that would tie multiple missions to a common well-defined geodetic reference frame (Beckley et al., 2007) and gravity field (Lemoine et al., 2010). Orbit testing at GSFC, has shown progressive improvement with increasingly refined POD modeling. Since 2009 GSFC has released six orbit series based on progressively improved POD standards: 1) the ITRF2005-based std0905, 2) the ITRF2008-based std1007 used previously in the MEaSURE's v1.0 product, 3) std1204 standards implemented in the MEaSURE's v2.0 product, 4) the ITRF2008-based std1504 standards implemented in the MEaSURE's v3.0 product, 5) the ITRF2014-based dpod2014 standards (Zelensky et al., 2017) implemented in the MEaSURE's v4.0 and v4.2 product, and now the std2006 orbit (Lemoine et al., 2020 (in progress)).

The std0905 SLR/DORIS dynamic radial orbit accuracies have been accessed at 1.5 cm (Lemoine et al., 2010, Zelensky et al., 2010). Since then updates to POD modeling standards have shown progressive improvement in orbit accuracy across all four missions. The latest standard, std2006, which includes improvements over a wide range of POD models (Table 3), shows accuracies of better than 1-cm for the Jason satellites and better than 1.5 cm for TP (Lemoine et al., 2020 (in progress)).

Although the GRACE/GRACE Follow-On(GFO)-derived gravity fields significantly improve the orbits from about 2005, the GRACE-derived TVG models do not accurately project back into the TOPEX era (Zelensky et al, 2012, Rudenko et al., 2014). To ensure consistency across missions we include TVG models derived from SLR/DORIS data across the missions. The std2006 gravity field includes the GSFC tvg0075 5x5 degree/order (d/o) bi-weekly terms estimated from 21 SLR/DORIS satellites spanning 1992.8 – 2020.4 The tvg0075 5x5 d/o terms supplement the background GOCO05s gravity field (Mayer-Guerr, 2015).

SLR/DORIS precise orbits were generated over the entire T/P, Jason-1, Jason-2 (or OSTM: (Ocean Surface Topography Mission), and Jason-3 mission time series based on the most recent std2006 POD standards. POD tests of the latest std2006 standards show improvement over the previous dpod2014 series (Table 4). Figure 4a illustrates the std2006 orbit improvement relative to dpod2014 over time using independent Crossover data. Although the std2006 orbits show increasing accuracy with time over the dpod2014, the mean radial differences over water show no significant trend. (Figure 4b).

These revisions to the precise orbit provide the geodetic consistency requirement necessary to tie T/P, Jason-1, Jason-2 (OSTM), and Jason-3.

Table 3. GSFC POD Model Standards spring 2020: std2006 (changes from dpod2014 in red) GEODYN version: 2002

Reference frame and displacement of reference points	
SLR	ITRF2014 slrf2014 (v200428); ILRS data handling: 2020-06-16 (with T2L2 corrections)
DORIS	ITRF2014 (dpod2014 (v4.0))
Earth tide	IERS2010
Ocean loading	GOT4.10 all stations
Atmosphere loading	none
CoM	GOT4.7 tidal variations, annual SLR-derived (Ries 2013)
Mean Pole	IERS2014 (linear)
EOP	IERS Bulletin A daily (consistent with ITRF2014); Diurnal and semi-diurnal variations in polar motion and UT1 due to ocean tides.
Precession / Nutation	IAU2000
Gravity	
Static	GOCO5S (from 6x6)
Time varying	tvg0075 5x5 d/o bi-weekly estimate boxcar-smoothed time series 1992.8-2020.4 from 21 SLR/DORIS satellites. Outside time series use linear, annual, semi-annual model from tvg0075 data. GOCO05s (from 6x6)
Atmospheric	90x90 3hr ECMWF GFZ
Tides	GOT4.10 50x50 (ocean); IERS2010 (Earth)

Satellite Surface Forces and attitude				
Albedo /IR	Knocke et al. (1988)			
Atmospheric drag	MSIS86			
Radiation pressure	**TOPEX**	**Jason-1**	**Jason-2**	**Jason-3**
	tuned 8-panel	tuned 10-panel	tuned 10-panel	tuned 10-panel
Radiation scale coeff.	C_R =pre-adj./arc	C_R =pre-adj./arc	C_R =pre-adj./arc	C_R =pre-adj./arc
Attitude	nominal: yaw model off-nominal: quaternions	quaternions / measured SAPA	quaternions / measured SAPA	quaternions / measured SAPA
Tracking data and parameterization				
Tracking data	SLR/DORIS (DORIS SAA: Jason1 corrected)			
Troposphere Refraction	SLR: Mendez-Pavlis; DORIS: VMF1			
Parameterization	Drag/8 hrs + opr along & cross-track /24 hrs + DORIS time bias /arc; 10-day arc dynamic solution			
DORIS modeling	DORIS beacon frequency bias modeling; beacon phase center			
Antenna reference	**TOPEX**	**Jason-1**	**Jason-2**	**Jason-3**
Satellite CoM	table	corrected table	table	table
SLR	LRA model	tuned offset, elevation model	tuned offset, elevation model	tuned offset, elevation model
DORIS	pre-launch offset, new Alcatel	pre-launch offset	tuned offset	tuned offset
SLR sigma weight	10-cm	10-cm	10-cm	10-cm
DORIS sigma weight	2-mm/s	3-mm/s down-weight SAA stations	$1/(\sin(elev))^{-1/2}$	$1/(\sin(elev))^{-1/2}$ down-weight SAA stations

Table 6. Evaluation of std2006 SLR/DORIS orbit performance for TP, J1, J2, and J3

Mission	orbit	average RMS residuals		
		DORIS (mm/s)	SLR (cm)	Xover * (cm)
TP cycles 12-343 Jan 1992 – Jan 2002	dpod2014	0.5265	1.689	5.638
	std2006	0.5256	1.667	5.640

J1 cycles 1-259 Jan 2002 – Jan 2009	dpod2014	0.3826	0.933	5.507
	std2006	0.3822	1.204	5.482
J2 cycles 1-303 Jul 2008 – Sep 2016	dpod2014	0.3829	1.021	5.312
	std2006	0.3896	1.205	5.285
J3 cycles 1-128 Feb 2016 – Aug 2019	dpod2014	0.4197	1.144	5.357
	std2006	0.4192	1.092	5.280
* altimeter crossover data are independent				

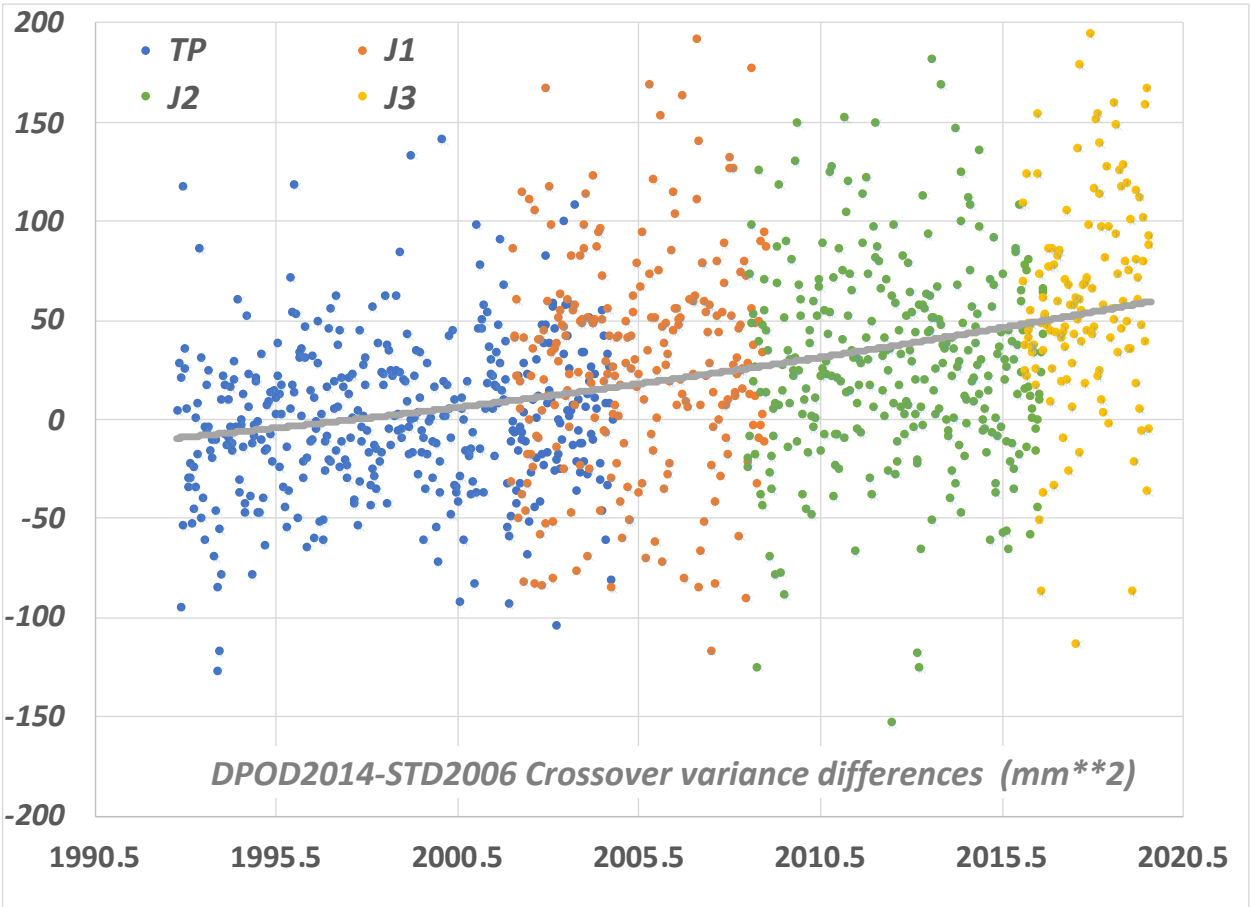

Figure 4a: std2006 radial orbit accuracy relative to dpod2014 using independent crossover data. Positive values indicate improvement derived from std2006.

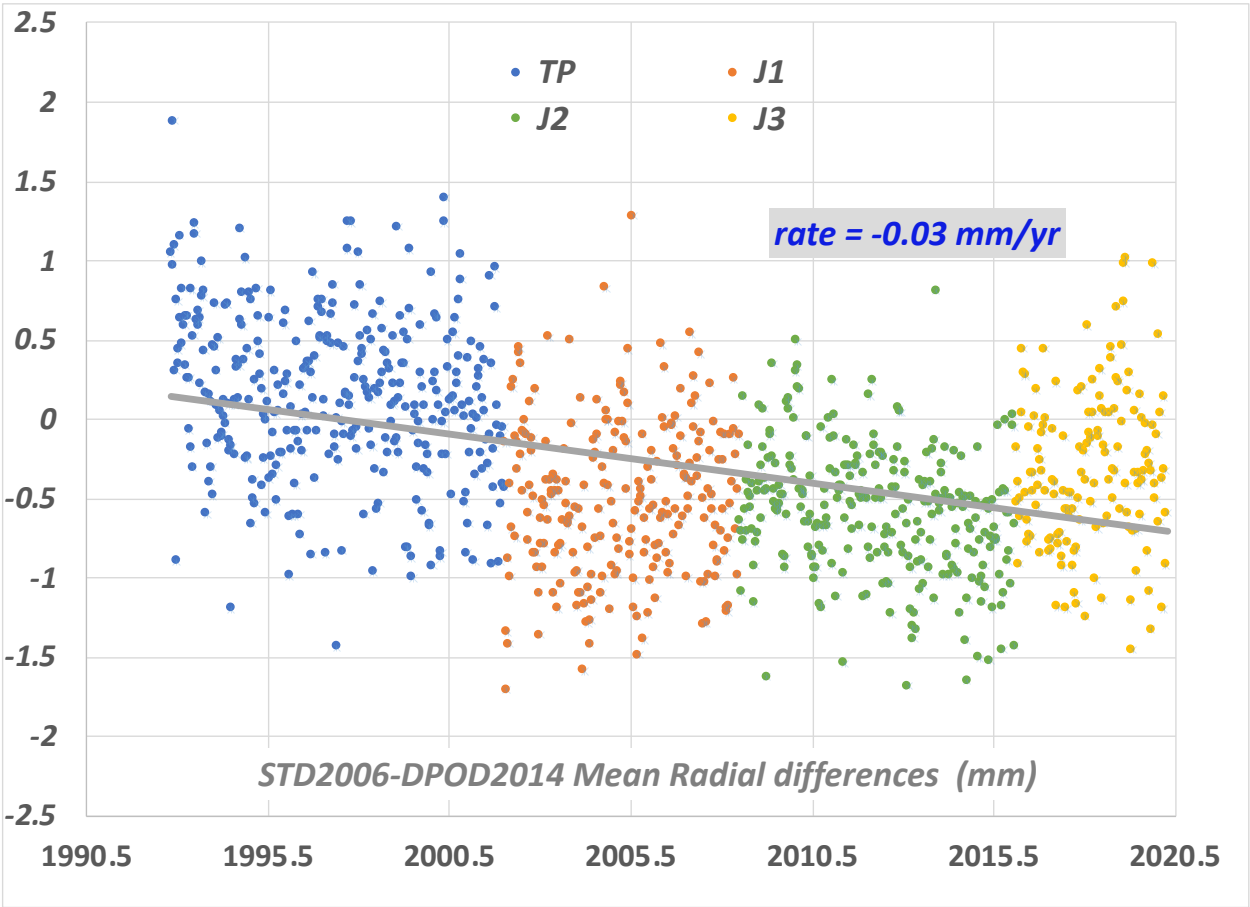

Figure 4b: **Mean radial std2006-dpod2014 orbit differences/cycle over water.**

2.1 Re-calibrated Jason-1 Microwave Radiometer (JMR)

Over the course of the Jason-1 mission several re-calibrations were performed to maintain and adhere to wet path delay (PD) stability/drift requirements (Brown, 2014). The most recent re-calibration is the end-of-mission climate quality calibration for the JMR (Brown, 2014) included in the GDR_E release. The end-of-mission re-calibration builds on previous calibrations, addresses remaining short term and long term residual calibration instability issues evident in the data (Figure 5a), and implements revised algorithms brought up to Jason-2 GDR_D standards.
To stabilize the long-term calibration, an inter-satellite calibration approach was applied. This approach essentially transfers the long-term calibration from other stable externally calibrated satellite microwave radiometers to the altimeter radiometers. The calibration standard in this case was chosen to be the SSM/I TB fundamental climate data record (FCDR) (Kummerow et al., 2010).

In addition to the long-term trend, JMR also exhibited time variable changes in calibration instrument temperature dependency. The effect is to introduce transient 60-day variations, which cannot be easily detected using the TB references, but is very apparent when comparing the geophysical retrievals to other references. A process was developed to infer the TB instrument temperature dependence over a 120-day moving window from comparisons of the path delay to the ECMWF model and the AMR wind speed to the altimeter wind speed. This correction was applied along with the long-term drift.
Finally, the JMR algorithms were updated to the Jason-2 GDR-D standard using the same processing software as is used for Jason-2 processing, but with coefficients specific to the JMR.
A drift correction has been applied to the final GDR_C calibration, which takes the form of a time variable scale and offset correction:

$$TB(ch,t)_{corrected} = TB(ch,t)_{uncorrected} - \Delta T_B(ch,t)$$

$$\Delta T_B(ch,t) = c_0(ch,t) + c_1(ch,t) TB(ch,t)_{uncorrected}$$

where the coefficients are derived by forcing agreement with the SSM/I Tb FCDR and on-Earth references (over the ocean (cold end) and over the Amazon rainforest (warm end)). The SSM/I FCDR was developed by Colorado State University (CSU) for NOAA and extends from 1987 to the present, covering the altimeter time period. The inter-satellite calibration provides a second independent reference (in addition to the natural reference method) and the demonstrated agreement between the two gives confidence in the observed long-term TB drift. Month-to-month calibration uncertainty is about 0.2°K (~2mm in PD). Estimated trend error (Figure 5b) can be computed as a function of record length:

- 2 mm/yr uncertainty for any 1 year
- < 1 mm/yr uncertainty for time spans greater than 2 years
- << 1 mm/yr for mission

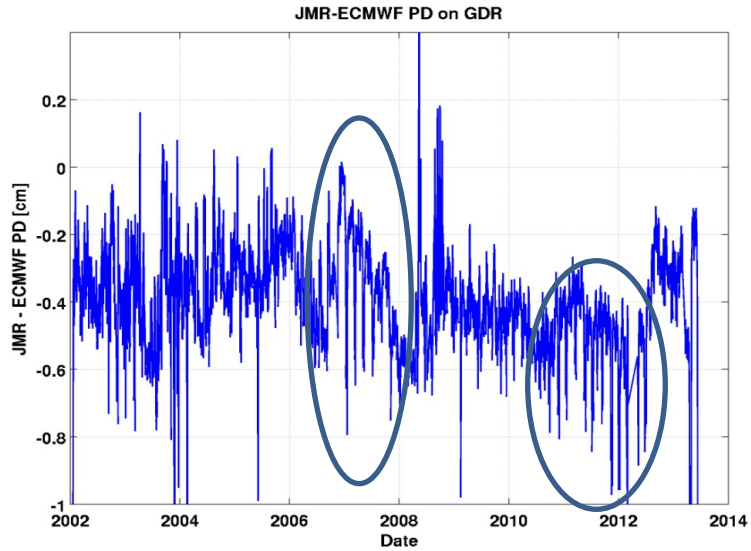

Figure 5a: JMR (GDR_C) minus ECMWF mean path delay differences detect times where further re-calibration is warranted.

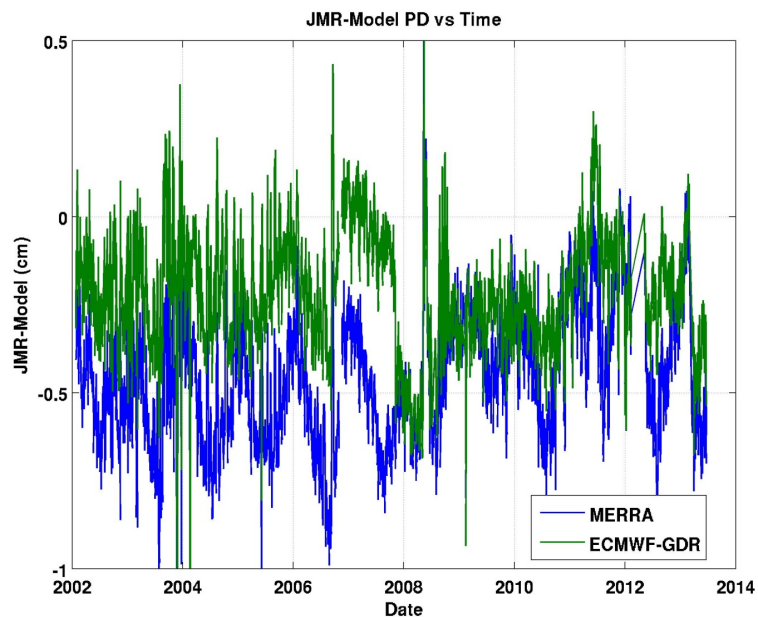

Figure 5b: Re-calibrated JMR versus MERRA and ECMWF model wet path delays suggest JMR drift rate less than 1mm/decade.

Several JMR algorithms were updated to Jason-2 AMR standards:

- All-weather sigma-0 attenuation correction algorithm
- Consistent sea ice and rain flagging
- Near land path delay retrieval algorithm

2.3 TOPEX Microwave Radiometer (TMR) Enhanced Wet Path Delays

The current GDR (MGDR_B) processing algorithm for TOPEX TMR uses a standard PD retrieval algorithm that underestimates path delay values near the coast due to land brightness temperature contamination. The application of a Mixed-Pixel algorithm Misra and Brown, 2011) non TOPEX TMR that has been has been successfully applied to the Advanced Microwave Radiometer (AMR) for Jason-2 and Jason-1 Microwave Radiometer (JMR) (Figure 6) to obtain coastal path delay values has been implemented. Algorithm performance on the TMR was compared with respect to the climate model MERRA (Figure 7) as well as JMR GDR processed PD values.

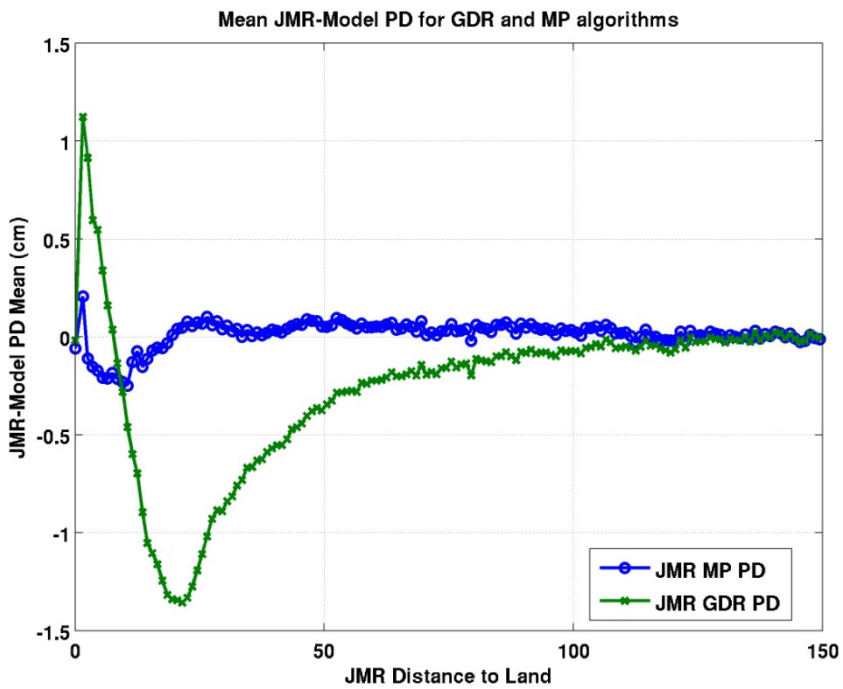

Figure 6: Enhanced GDR_E JMR path delays recovered near land via mixed pixel (MP) algorithms provide improved accuracies in coastal areas.

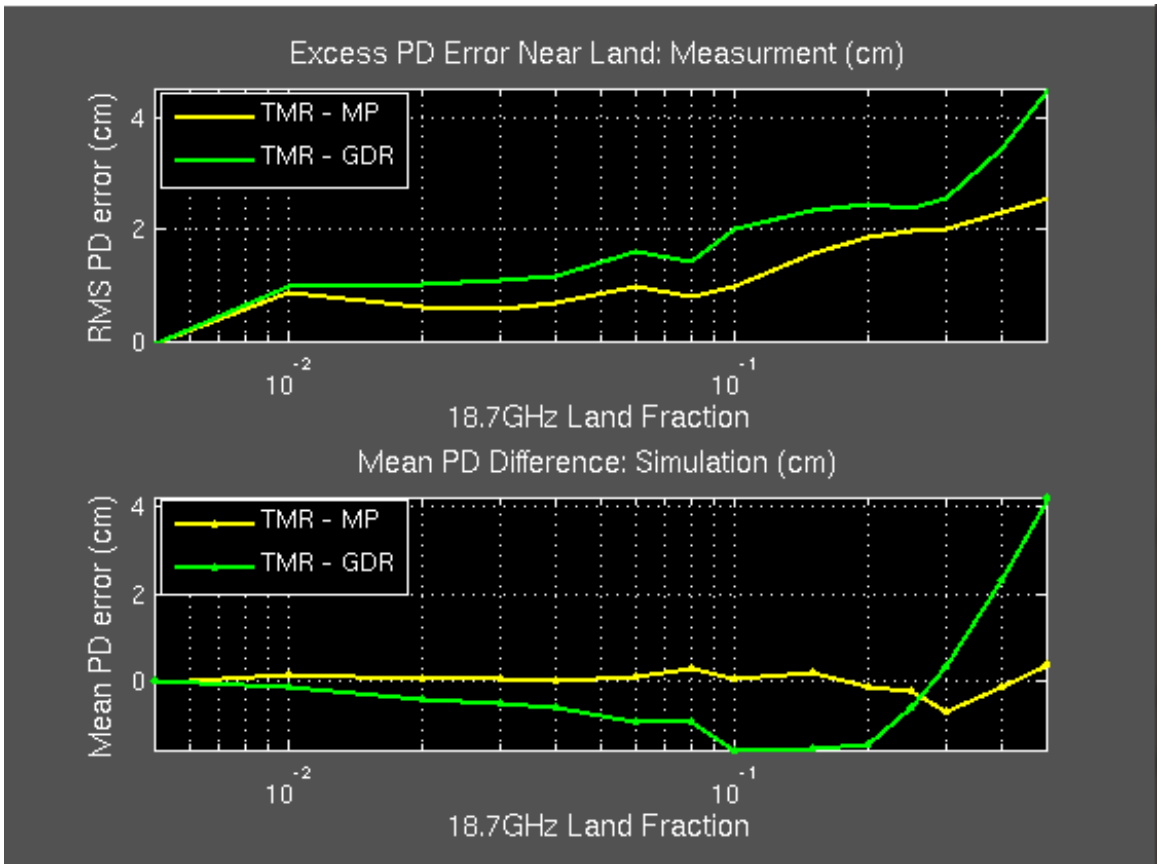

Figure 7: The MP algorithm successfully compensates for land contamination. The figures above show the performance of the MP algorithm in terms of mean difference and RMS error with respect to MERRA. As observed, the GDR algorithm retrieved PDs have a characteristic dip as the land fraction increases. This is due to an increase in the 18GHz Tb that is not offset by increase in the higher frequency Tbs. The mixed pixel algorithm clearly has lower mean difference and RMS error compared to the GDR algorithm.

2.4 Ocean Tide Corrections

The corrections for short-period (diurnal and faster) tides applied to TOPEX/Poseidon are based on GOT4.8, and those for Jason-1&2 are based on GOT4.10. The GOT4.8 model is derived from T/P altimetry only, while the GOT4.10 model is derived solely from Jason-1&2 altimetry. Model selection was based on accuracy assessments via comparisons to an improved bottom-pressure validation network (Stammer et al., 2015), and to the efficacy of the models to mitigate 59-day oscillations in altimetric global mean sea level (e.g., Masters et al., 2012). These are caused in part by errors in the S2 tide correction (the alias period of S2 is 59 d), as well as errors in anything correlated with solar forcing (radiation pressure, satellite thermal flexures, etc.), including the satellite center-of-gravity (Cg) correction. Unfortunately, it is now clear that at the level of 5-10 mm (roughly the amplitude of the 59-day oscillations in mean sea level), the T/P and Jason altimeters are inconsistent at the S2 frequency (Figure 8).

The model for long-period ocean tides is described by Ray & Erofeeva (2014). It is a hydrodynamic solution of the long-period tidal equations, formally unconstrained by observations but fine-tuned to agree with measurements of the fortnightly Mf tide, including measurements of Mf polar motion and length of day. Five dynamic constituents are given explicitly (Sa, Ssa, Mm, Mf, and Mt, with periods from 1 year to 9 days). The prediction software automatically infers five additional constituents, and it applies standard nodal adjustments to all lunar constituents. A final

constituent is included for the node tide (period 18.6 y), which takes a (self-consistent) equilibrium form. The model for the M2 internal tide derived empirically from satellite data without reliance or knowledge of wave dynamics or ocean stratification is described by Ray and Zaron (2016)..

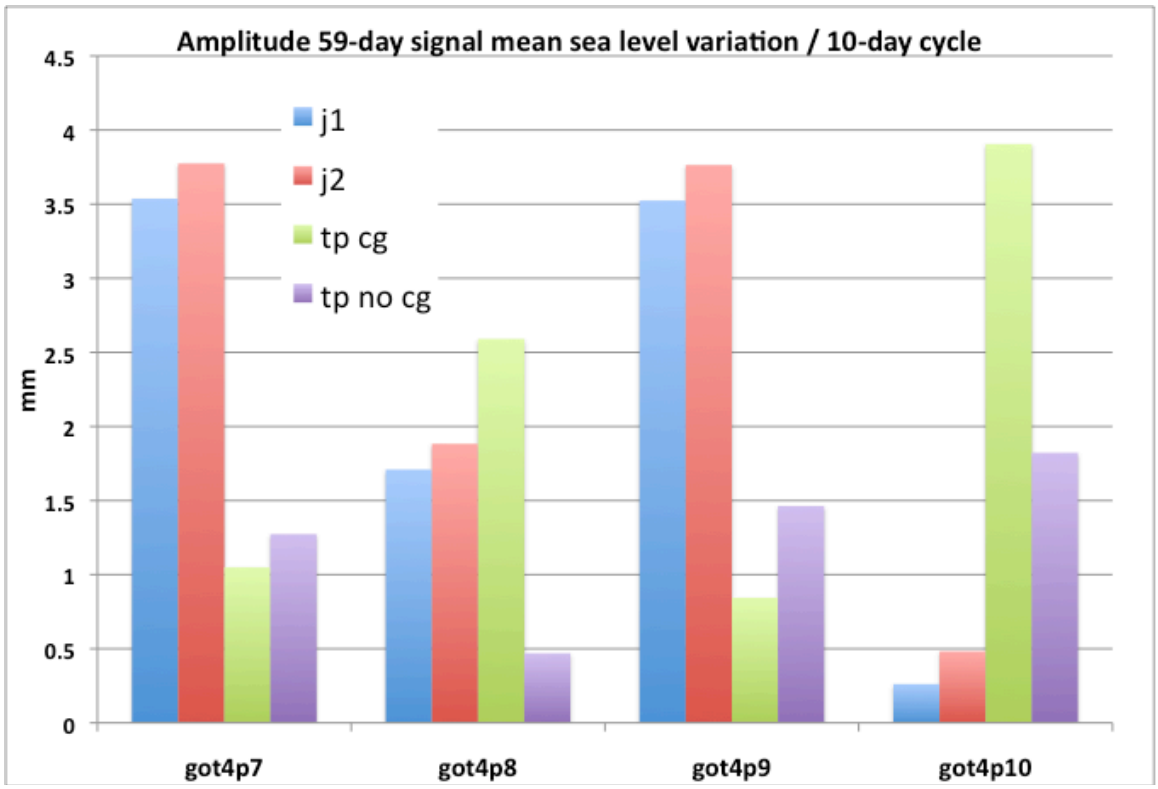

Figure 8: The resultant amplitude of the 59-day signal that varies in T/P, Jason-1, and Jason-2 GMSL estimates with the application of ocean tide model, and the application of Cg to T/P altimetry.

2.5 Pole Tide Correction

A revised pole tide correction has been developed (Desai et al., 2015) that replaces the earlier model contained in the T/P and Jason GDRs. The two primary revisions to the earlier model include 1) "upgrading to a self-consistent equilibrium model for the displacement of the ocean surface relative to the Earth's crust and explicitly modeling the load pole tide with respect to the CM", and 2) "that pole tide displacements for altimetry be computed from residual polar motion with respect to a drifting mean pole, with the rate determined from almost 80 years of observations (Argus and Gross, 2004)". The impact on global mean sea level estimates is negligible due to geographical cancellation of signal. Impact on regional sea level estimates range from ±0.25 mm/y (Figure 9).

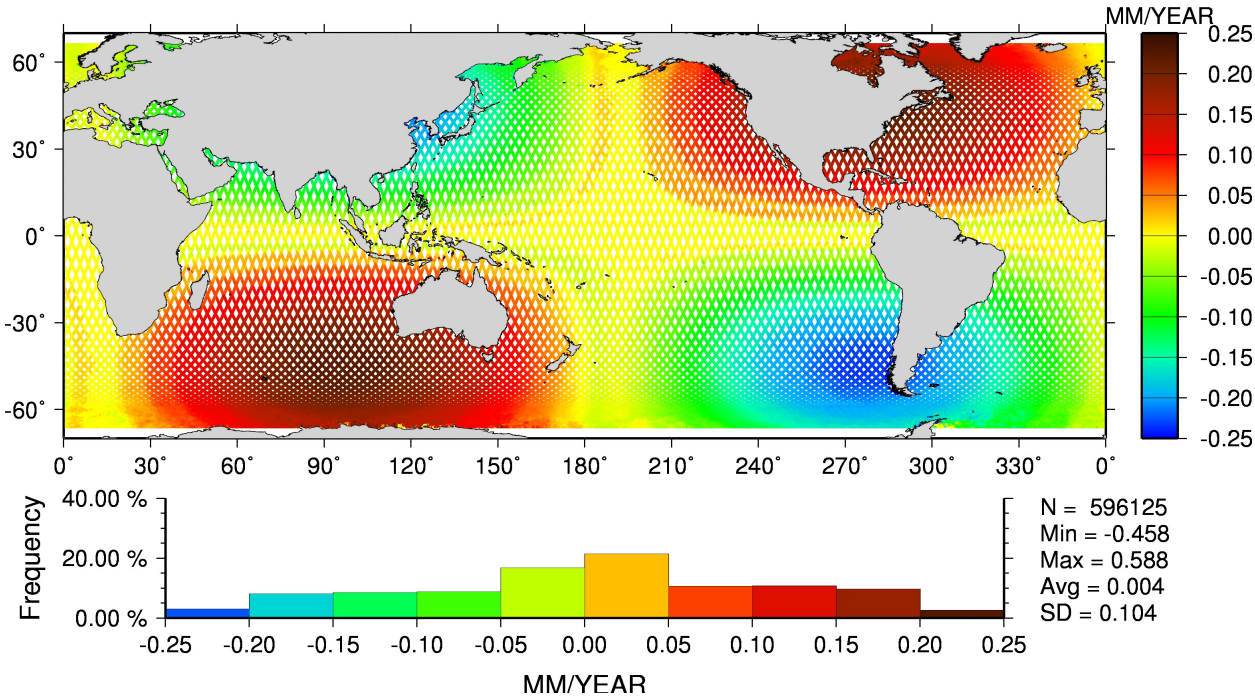

Figure 9: Regional linear trends of pole tide differences between revised model (Desai, et al., 2015) and previous model contained in mission GDRs. The impact on regional sea level is at the level of +/- 0.25 mm/y.

2.6 Mean Sea Surface

The DTU15 mean sea surface (Andersen, 2015.) replaces the DTU13 surface as the reference for the SSH anomalies, and for the generation of the cross-track gradient correction derived from the regional slopes at each geo-referenced location. Additional altimetry derived from a 22+ year record and the inclusion of the Jason-1 geodetic mission data and CryoSat-2 data are incorporated in the generation of the DTU15 surface. Revised cross-track slopes based on the DTU15 MSS are shown in Figure 10.

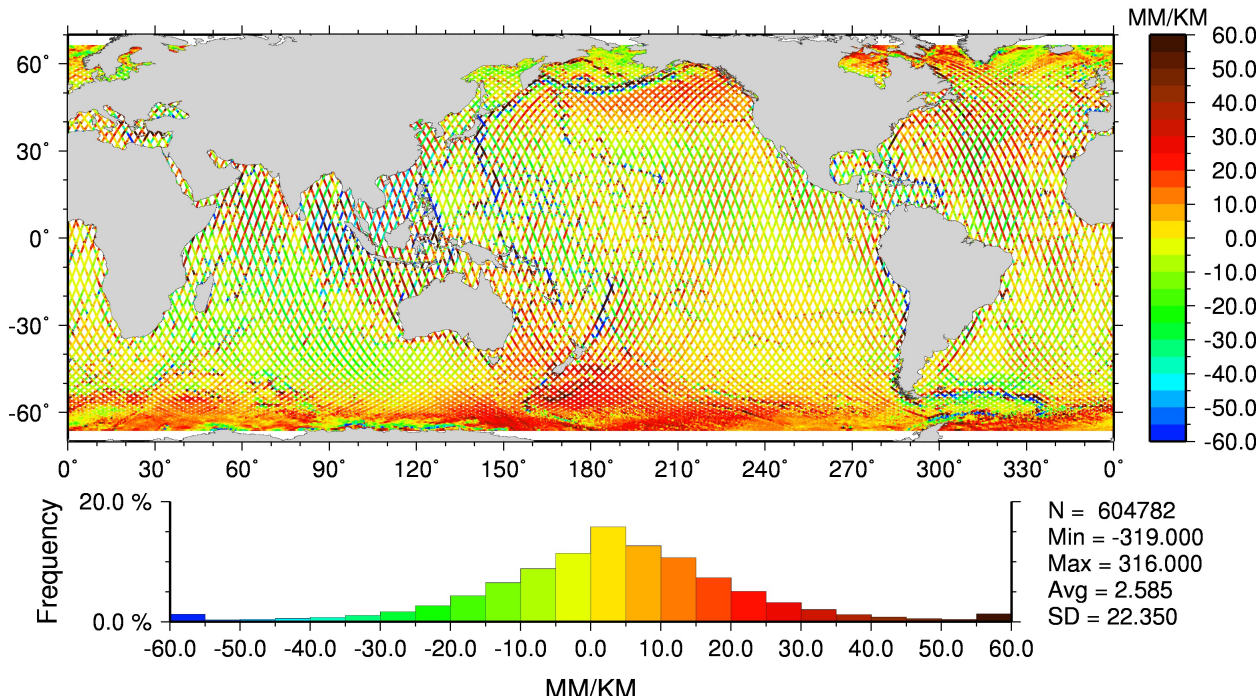

Figure 10: Cross-track slopes evaluated at geo-referenced locations over ocean based on DTU15 MSS.

3.0 Inter-mission biases

3.1 Sea State Bias

In an effort to adhere to inter-mission consistency and provide a homogeneous SSH time series, the non-parametric (NP) sea state bias models that have evolved over time based on the works of Gaspar et al., 1998, 2002, Labroue et al., 2004, and most recently Tran et al., 2010&2012 have been employed to correct for sea state bias effects on the TOPEX, Jason-1&2 altimeters. Continuous improvements to these empirical based models has been due in part to improved POD strategies based on consistent geophysical modeling strategies and a single terrestrial reference frame adopted across all missions (Lemoine, et al, 2010), adoption of a consistent ground reprocessing strategy (4-parameter Maximum Likelihood Estimator (MLE4) re-tracking, Amarouche et al., 2004), improved atmospheric load corrections (Carrère and Lyard, 2003), and revised 2-parameter wind speed algorithms specifically tuned for TOPEX (Gourrion et al., 2002), and Jason-1 (Collard, 2004) altimeters. The specific SSB tables implemented for each mission are identified in Appendix II and can be obtained from AVISO.

A collaborative effort with Dr. Ngan Tran from CLS has produced non-parametric (NP) solutions for TOPEX (Side A and B) derived from collinear SSH residuals based on revised GSFC std0809 ITRF2005 (Eigen-GL04c) replacement orbits, and current correction algorithms outlined in Table 2 (Tran et al, 2010). Improved agreement between TOPEX and Jason-1 is realized with the application of the NP model as compared to results based on a revised parametric model derived from crossover residuals (Beckley, et al 2010). Comparison of the two models via SSH collinear differences (based on TPJAOS v1.0) shows an approximate +3mm Side A bias and -4.5mm Side B bias and an annual signature of 1mm in amplitude of the mean difference (Figure 11).

Rectification of the approximate overall 6-8 mm Side A/B bias is accomplished by comparing the altimeter derived SSH variations to the height variations from a near global network of tide gauges (see Tide Gauge Validation section below).

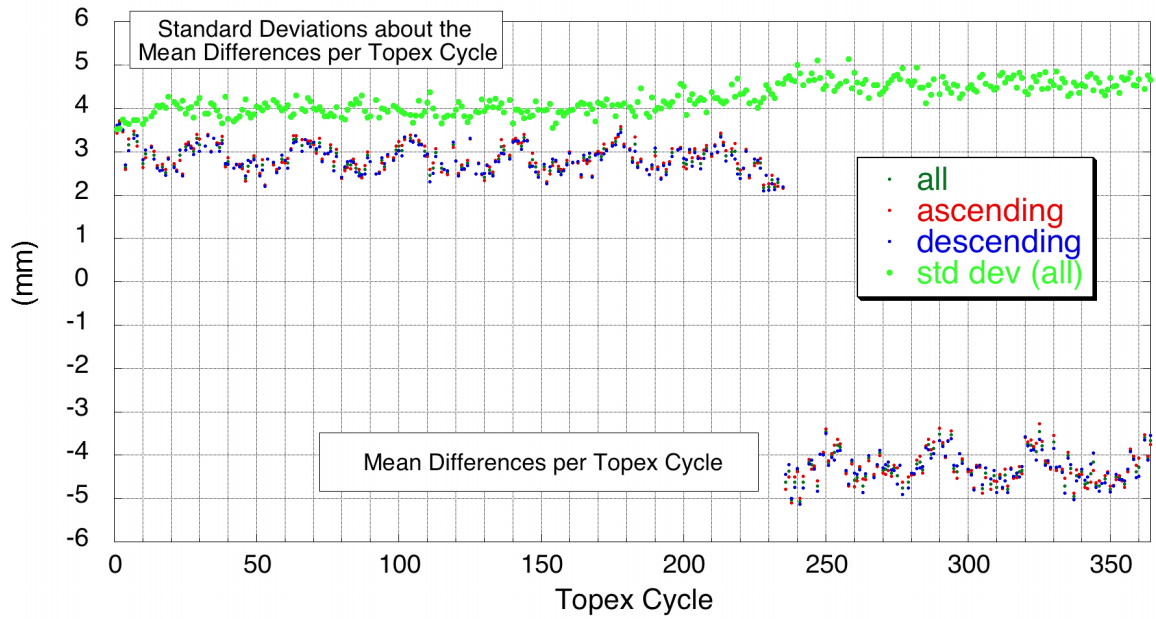

Figure 11: Mean differences of sea surface height between heights based on parametric versus non-parametric sea state bias solutions reveals separate biases (Chambers et al., 2003) for TOPEX Side A (cycles 1-235) and for Side B (cycles 236-364).

3.2 Jason-1, 2, & 3 Verification Phase Results

A critical component to providing credible mean sea level estimates from integrated multiple altimeter missions is the accurate determination of inter-mission biases. The verification campaigns during the roughly first 6 months of the Jason-1, 2, and 3 missions provided essential near-simultaneous altimeter observations that would enable the seamless transition from T/P to Jason-1 to Jason-2 to Jason-3.

Figures 12, 13, and 14 show the estimated global mean bias between TOPEX/Jason-1, Jason-1/Jason-2, and Jason-2/Jason-3 respectively derived from regional mean variations of the SSH collinear differences of the near-coincident measurements over the time period of the verification phase(s). All pertinent range and geophysical corrections are applied in order to identify and isolate any regional residual differences/errors attributed to any remaining unavoidable inter-mission inconsistencies. Each figure shows some expected regional variance in the estimate of the global mean bias estimate, though each estimate has a very normalized distribution of SSH mean residuals with a standard deviation not exceeding 2 mm.

After several range correction omission errors were accounted for in the Jason-1 GDR_E and Jason-2 GDR_D, the Jason-1/2 inter-mission bias is nearly zero (Figure 13), thus a bias of 24.1 mm (23.9 + 0.2 mm) is applied to TOPEX (Side B) to align to the Jason-1/2 reference datum. The Jason-2/Jason-3 bias shown in Figure 20 shows Jason-3 SSH to be 29.0 mm lower than Jason-2.

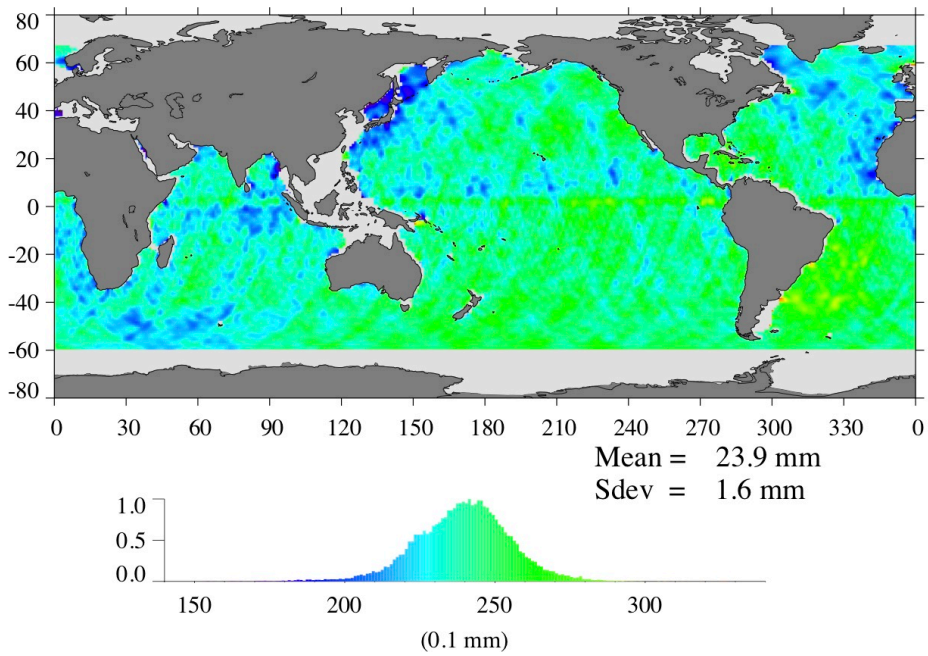

Figure 12: v5.0 Jason-1 minus TOPEX (Alt B) inter-mission bias is estimated from averaged SSH collinear residuals during the Jason-1 verification phase. Color scale is +/- 1cm about estimated mean.

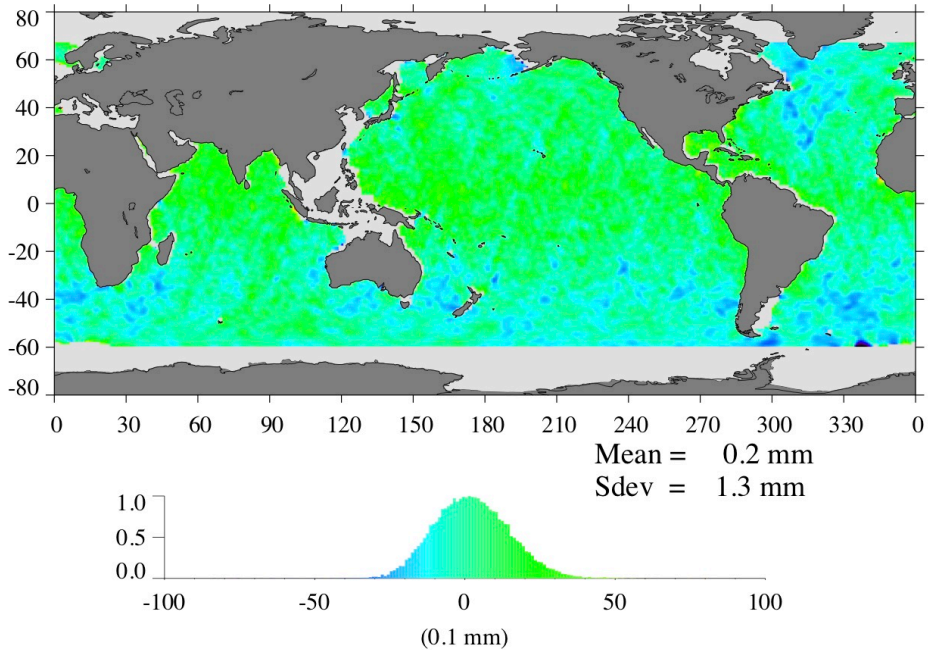

Figure 13: v5.0 Jason-2 minus Jason-1 inter-mission bias is estimated from averaged SSH collinear residuals during Jason-2 verification phase. Color scale is +/- 1cm about estimated mean.

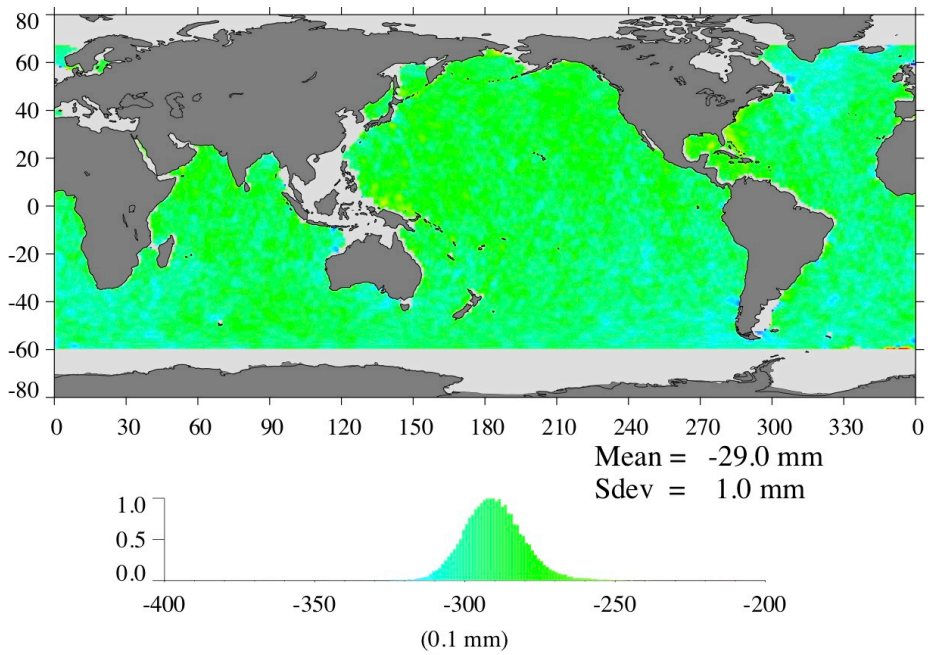

Figure 14: v5.0 Jason-3 minus Jason-2 inter-mission bias is estimated from averaged SSH collinear residuals during Jason-3 verification phase. Color scale is +/- 1cm about estimated mean.

3.3 Tide Gauge Validations

Validation procedures are regularly performed by Prof. Gary Mitchum by comparing altimeter derived SSH variations to height variations measured from a global network of tide gauges (Mitchum, 2000). From the beginning of the TOPEX/Poseidon (T/P) mission, methods to estimate altimeter drift from comparisons with the global tide gauge network have continuously evolved, (for example, as the SSH time series approached two decades, questions about the handling of long period tides, particularly the Msf and Mf components, were raised and we adapted our methods appropriately) first in a research mode with NASA funding (primarily the T/P and OST SWTs and later from MEaSUREs), and later becoming general and operationally-oriented.

Validation results shown here are based on the current near-global network of 64 sites (Figure 15). The largest uncertainty in estimated rates derived from the gauges arises from land motion at the sites. Vertical land motion corrections based on the latest ULR6 (University of La Rochelle Consortium) GPS velocity fields (Santamaría-Gómez et al., 2012, Wöppelmann et al., 2009) have been implemented.

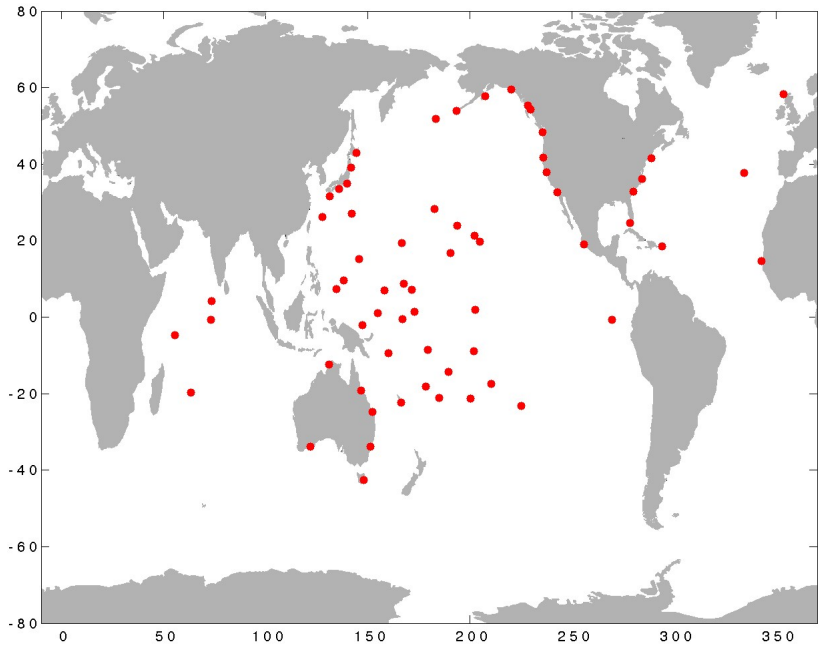

Figure 15: Current network of 64-tide gauge sites (red dots).

The tide gauge validation analysis tools currently in place evaluates and monitors within-mission stability, and provides an assessment of inter-mission bias estimates (Ray et al., 2010, Leuliette and Scharoo, 2010, Nerem, et al., 2018). As shown in figures 12, 13, and 14 TOPEX/Jason-1, Jason-1/Jason-2 (J1/J2), and Jason-2/Jason-3 inter-mission biases can be evaluated globally by direct SSH collinear differencing benefiting from the dedicated verification phases. The TOPEX Side A and Side B altimeters are treated as if separate missions as is noted in the independent evaluation of the sea state bias for each altimeter. There is no Side A/B coincident overlapping data available thus we are reliant on the tide gauge network to estimate this particular "inter-mission" bias. Figure 16 shows an estimated Side A/B bias of 6.7 mm resultant to differences in mean variations to a common Jason-1/2 reference level datum (Nerem et al., 2018). An adjustment to Poseidon-1 SSH is applied to account for an estimated bias of 27.8 mm (no retracking before cycle 132), and 22.1 mm after cycle 132 (retracked) with respect to TOPEX adjusted to J1/J2 reference level. The TOPEX/Poseidon-1 bias is estimated by computing the mean of T/P open-ocean collinear SSH residuals (figure 17).

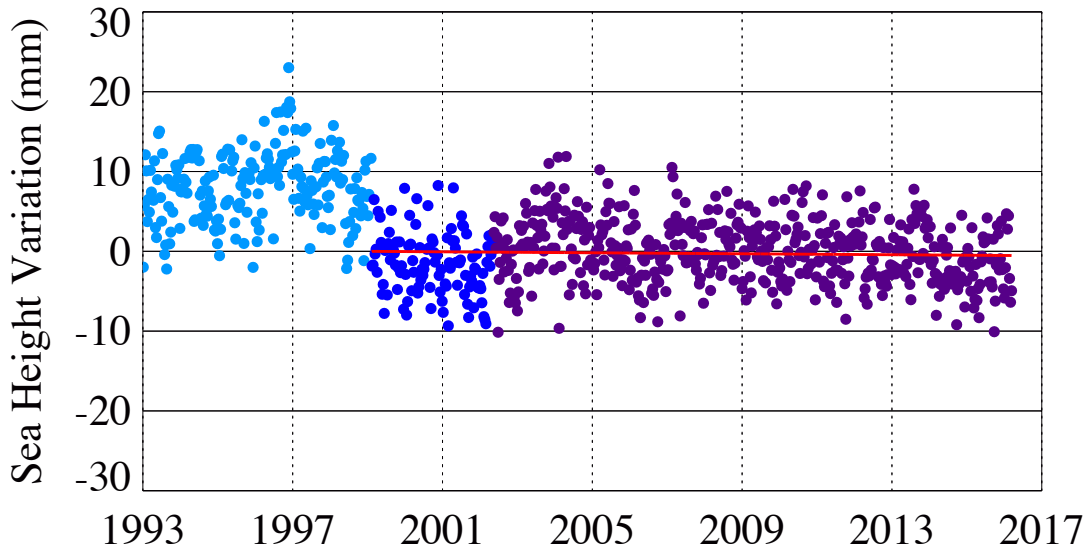

Figure 16: Estimate of v5.0 TOPEX Side A/B bias is derived from per cycle mean comparisons of altimeter SSH variations with height variations from 64-site tide gauge network. The TOPEX data (both Side A (light blue dots) and Side B (dark blue dots)) have been adjusted by 24.1 mm as derived from collinear residuals (Jason-1 minus TOPEX Side B =23.9 mm, Jason-2 minus Jason-1 =0.2 mm) from the Jason-1and Jason-2 verification phases. An additional -6.7 mm bias is estimated to align TOPEX Side A to Side B and the J1/J2 reference level datum.

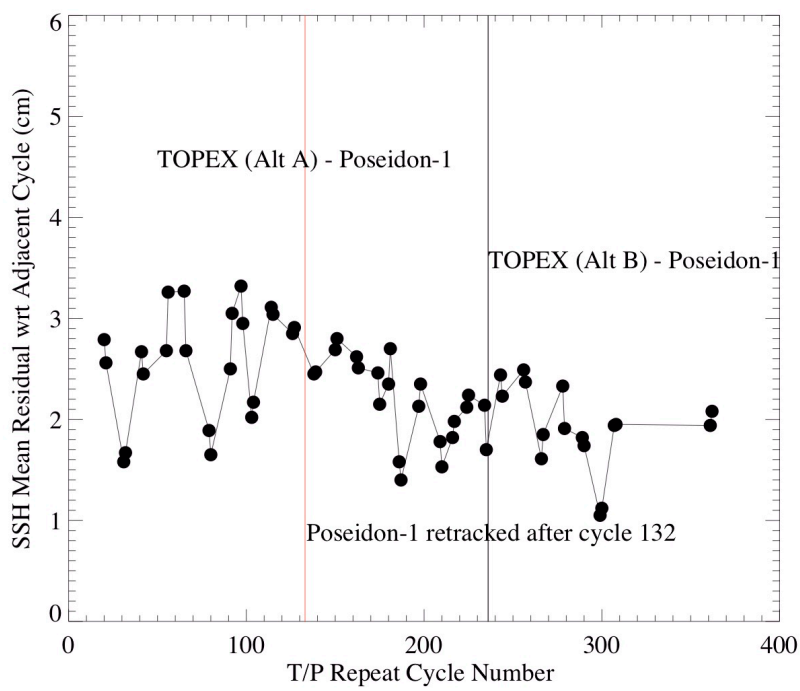

Figure 17: Poseidon-1 bias with respect to adjusted v5.0 TOPEX (wrt J1/J2 reference level) is estimated via mean collinear TOPEX minus Poseidon-1 SSH residuals. Before cycle 132, Poseidon-1 data is not retracked.

To assess the inter-mission consistency and stability of the entire 27-year time series, the TOPEX A/B bias, and the adjustment biases to Jason-1 and Jason-3 that were derived from their

verification campaign SSH collinear residuals are applied, and compared against a high-fidelity 64-site tide-gauge network as a "single mission" time series. These tide gauge comparisons provided in Figure 18 show per cycle mean differences to be predominantly within a ± 1.0 cm envelope, and to have an overall estimated "drift" rate of -0.03 mm/y with a standard deviation of the mean differences to the linear fit of 4.2 mm.

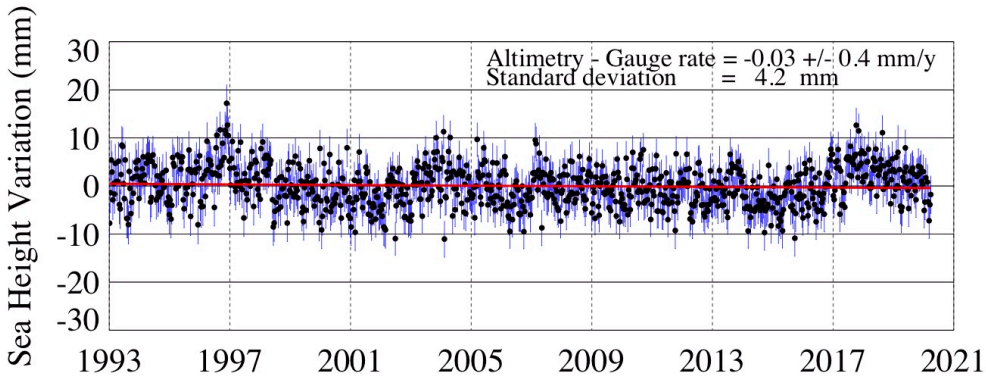

Figure 18: Resultant per cycle comparisons of altimeter derived v5.0 SSH variations with height variations from 64-site tide gauge network after application of inter-mission biases to form a single adjusted SSH Climate Data Record.

4.0 Estimation of Global and Regional Mean Sea Level

Global and regional mean sea level variations derived from the TPJAOS v5.0 product are shown in Figures 19 through 21 below. Details of the derivation of the sea level estimates are provided in Beckley et al., 2007 and 2010. The examples below do have the glacial isostatic adjustment (GIA; Peltier 2009) applied; annual and semi-annual signals are intact in Figure 19, and have been removed in Figures 20 and 21. The edit strategy employed based on the quality flag word bits edited observations where any one of bits 1, 3-4, 9-14 where set to 1, or bits 7 and 8 both set to 1 (see Appendix). Observations where the terrain type is not equal to zero indicating non open-ocean are edited. The regional sea level trends though do include coastal SSH trend estimates.

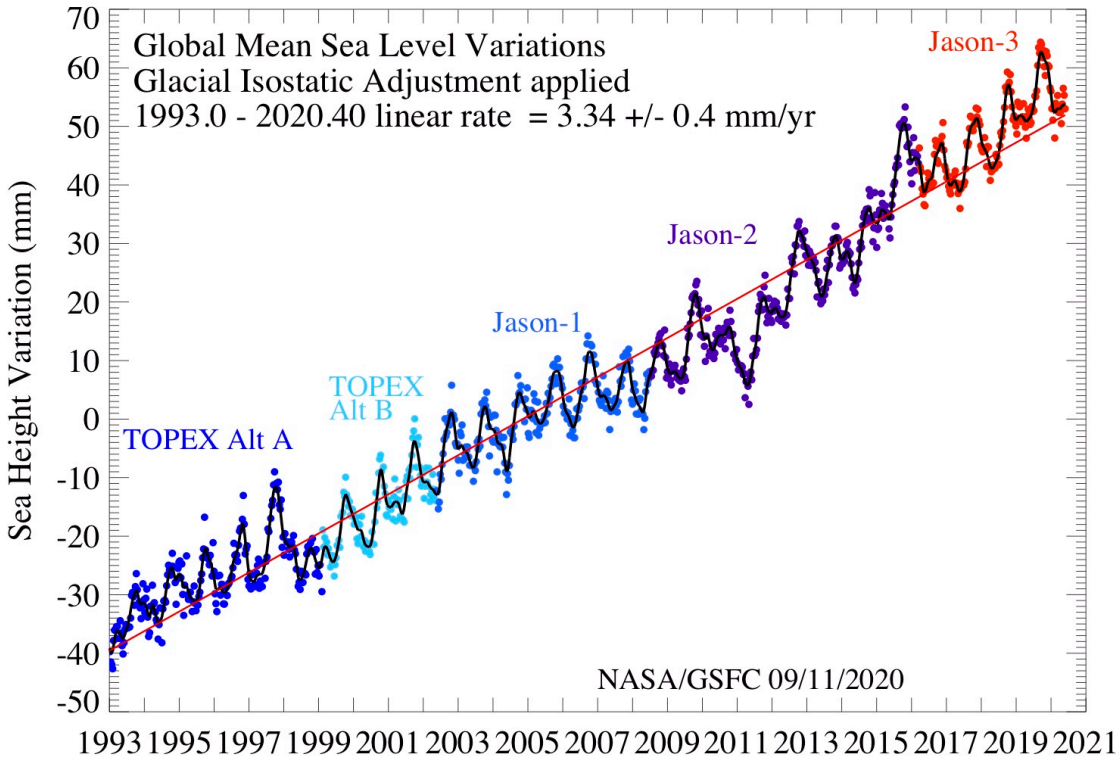

Figure 19: Global mean sea level is estimated at 3.34 ± 0.4 mm/yr (GIA applied) based on SSH variations with respect to 20-year TOPEX/Jason mean profile. Sea surface heights are based on cycles 11-1020 of TPJAOS v5.0 SSH anomaly product. Black line denotes SSH variation after application of 60-day Hanning filter.

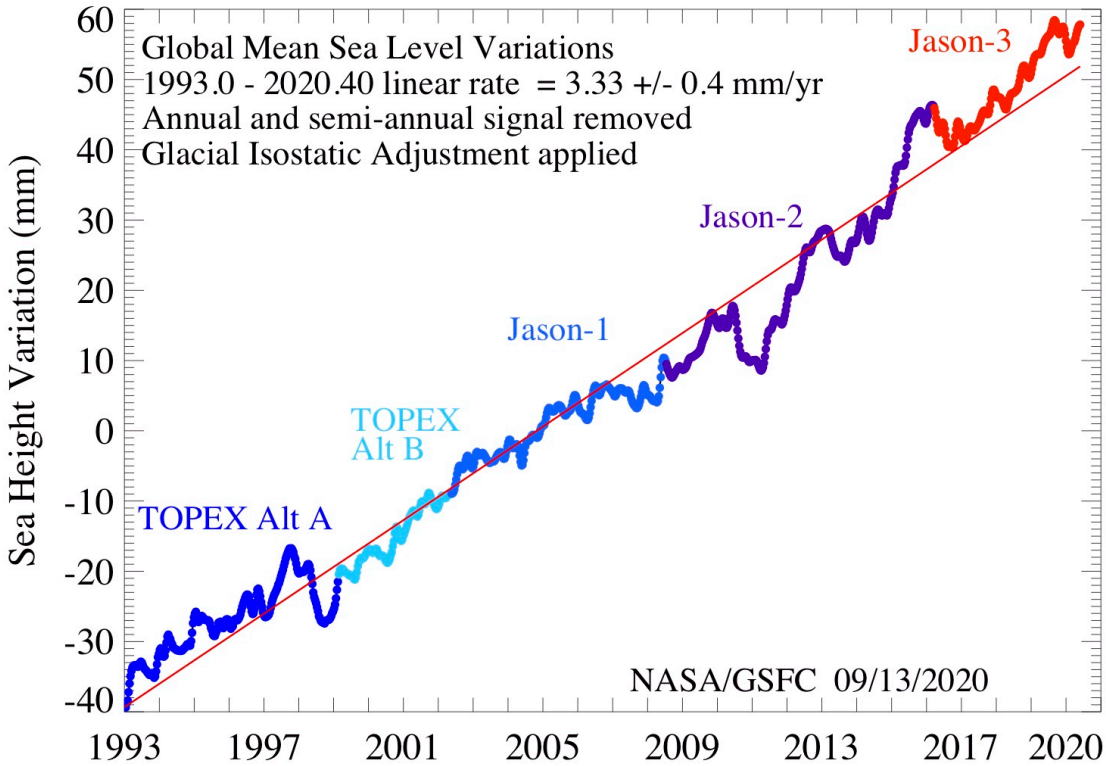

Figure 20: **Global mean sea level variations estimated as in Figure 22 with annual and semi-annual signal removed.**

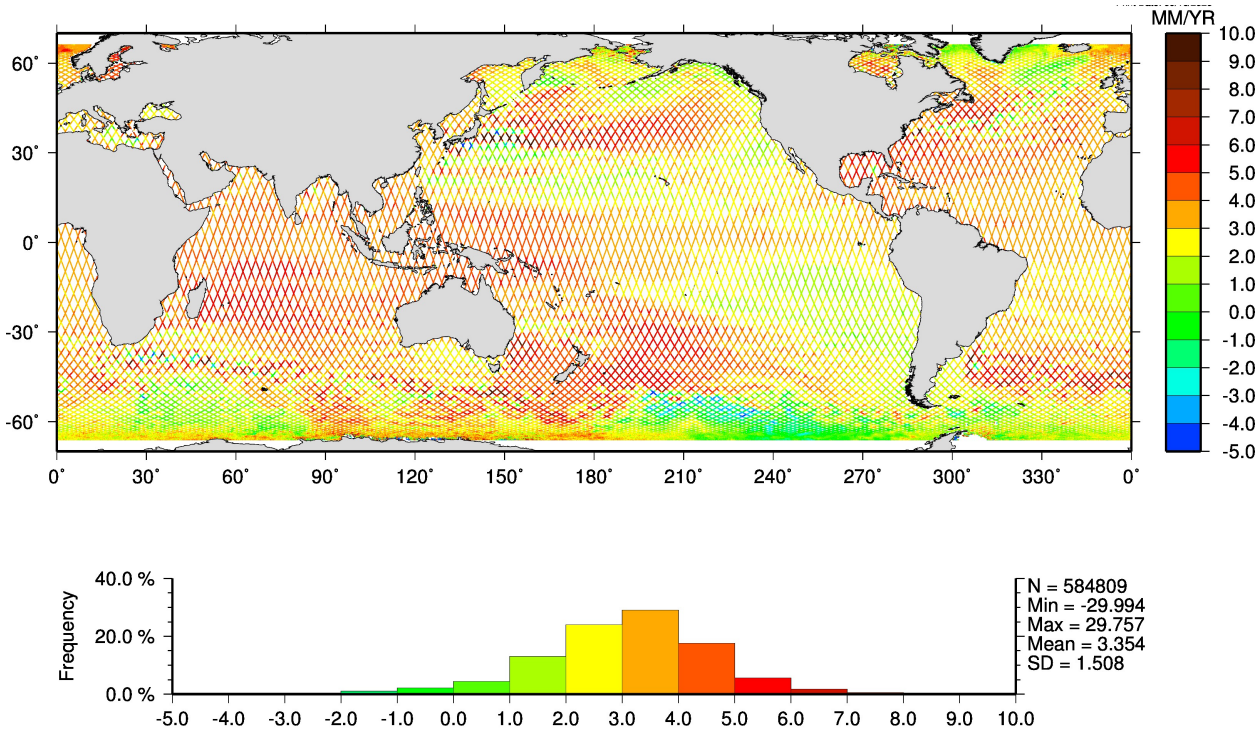

Figure 21: Regional mean sea level variations (GIA applied, annual and semi-annual signal removed) at each geo-referenced location are based on cycles 11-1020 of the TPJAOS v5.0 SSH anomaly product.

5.0 References

Ablain, M., A. Cazenave, G. Valladeau, et al., A new assessment of the error budget of global mean sea level rate estimated by satellite altimetry over 1993–2008, Ocean Sci., 5, 193–201, 2009.

Ablain, M., Cazenave, A., Larnicol, G., et al., 2015. Improved sea level record over the satellite altimetry era (1993–2010) from the Climate Change Initiative project. Ocean Sci. 11 (1), 67–82. http://dx.doi.org/10.5194/os-11-67-2015.

Altamimi, Z., P. Rebischung, L. Metivier, and C. Xavier (2016), ITRF2014: A new release of the International Terrestrial Reference Frame modeling nonlinear station motions, J. Geophys. Res. Solid Earth, 121, doi:10.1002/2016JB013098.

Amarouche L., P. Thibaut, O.Z. Zanife, P. Vincent, and N. Steunou. 2004. Improving the Jason-1 ground retracking to better account for attitude effects. *Marine Geodesy*, 27(1-2) :171-197.

Andersen, O. B., G. Piccioni, L. Stenseng, and P. Knudsen, The DTU15 Mean Sea Surface and Mean Dynamic Topography-focusing on Arctic issues and development., 2015 Ocean Surface Topography Science Team Meeting, Reston, VA, USA.

Argus DF, Gross RS (2004) An estimate of motion between the spin axis and the hotspots over the past century. Geophys Res Lett 31. doi:10.1029/2004GL019657

Beckley, B.D., N.P. Zelensky, S.B. Luthcke, and P.S. Callahan. 2004. Towards a seamless transition from TOPEX/Poseidon to Jason-1. *Marine Geodesy,* 27, 373-384.

Beckley, B.D., F.G. Lemoine, S.B. Luthcke, R.D. Ray, and N.P. Zelensky. 2007. A reassessment of TOPEX and Jason-1 altimetry based on revised reference frame and orbits. *Geophys. Res. Lett.*, 34, L14608, DOI:10.1029/2007GL030002.

Beckley, B.D., N.P. Zelensky, S.A. Holmes, F.G. Lemoine, R.D. Ray, G.T. Mitchum, S. Desai, S.T. Brown, Assessment of the Jason-2 Extension to the TOPEX/Poseidon, Jason-1 Sea-Surface Height Time Series for Global Mean Sea Level Monitoring, *Marine Geodesy*, 33(S1): 447-471, 2010, Supplemental Issue on OSTM/Jason-2 calibration/validation, Vol. 1, DOI: 10.1080/01490419.2010.491029.

Beckley, B. D., Callahan, P. S., Hancock, D. W., Mitchum, G. T., & Ray, R. D. (2017). On the "cal-mode" correction to TOPEX satellite altimetry and its effect on the global mean sea level time series. Journal of Geophysical Research: Oceans, 122. https://doi.org/10.1002/2017JC013090.

Benada, J. R., 1997. "*PO.DAAC Merged GDR (TOPEX/POSEIDON) Generation B User's Handbook"*, Version 2.0, JPL D-11007.

Brenner, A. C., C. J. Koblinsky, and B. D. Beckley. 1990. A Preliminary Estimate of Geoid-Induced Variations in Repeat Orbit Satellite Altimeter Observations. *J. Geophys. Res.,* 95(C3), 3033- 3040.

Brown, S., S. Desai, N. Lahaye, The End-of-Mission Climate Quality Calibration for the JMR, 2014 Ocean Surface Topography Science Team Meeting, Konstanz, Germany, http://meetings.aviso.altimetry.fr/fileadmin/user_upload/tx_ausyclsseminar/files/28Ball1400-3_OSTST_14_JMR_calibration_Brown.pdf

Carrère, L., and F. Lyard. 2003. Modelling the barotropic response of the global ocean to atmospheric wind and pressure forcing. *Geophys. Res. Lett.,* 30(6), art. 1275, DOI:10.1029/2002GL016473.

Cazenave, A., D.P. Chambers, P. Cipollini, L.L. Fu , et al., Sea Level Rise Regional And Global Trends, OCEANOBS2009- Plenary Paper (2009).

Collard F. and S. Labroue (2004), New Wind Speed Algorithm for Jason-1, Poster presented at the *OSTST Meeting*, November 2004, St Petersburg, Florida, USA.

Chambers, D.P., S.A. Hayes, J.C. Ries, T.J. Urban. 2003. New TOPEX Sea State Bias Models and their Effect on Global Mean Sea Level. *J. Geophys Res*., 108, 3305.

Desai, S., J. Wahr, B. Beckley, Revisiting the pole tide for and from satellite altimetry, Journal of Geodesy, 89(8), 747-842, 2015. DOI 10.1007/s00190-015-0848-7

Fasullo, J.T., Nerem, R.S., Hamlington, B., 2016. Is the detection of accelerated sea level rise imminent? Sci. Rep. 6, 31245. http://dx.doi.org/10.1038/srep31245.

Gaspar, P., F. Ogor, P. Y. Le Traon, and O. Z. Zanife (1994), Estimating the sea state of the TOPEX and Poseidon altimeters from crossover differences, J. Geophys. Res., 99, 24,981 – 24,994.

Gaspar, P., and J.-P. Florens. 1998. Estimation of the sea state bias in radar altimeter measurements of sea level: Results from a new nonparametric method. *J. Geophys. Res.* 103:15803-15814.

Gaspar, P., S. Labroue, F. Ogor, G. Lafitte, L. Marchal, and M. Rafanel. 2002. Improving nonparametric estimates of the sea state bias in radar altimeter measurements of sea level. *J. Atmos. Oceanic Technol.* 19:1690-1707.

Gourrion, J., D. Vandemark, S. Bailey, B. Chapron, G. P. Gommenginger, P. G. Challenor, and M. A. Srokosz (2002), A two-parameter wind speed algorithm for Ku-band altimeters, J. Atmos. Oceanic Technol., 19, 2030 – 2048.

Picot, N., et al., 2016, Jason-1 Products Handbook, References: CNES : SALP-MU-M5-OP-13184-CN JPL : JPL D-21352 Issue: 5 rev 1 Date: April 4th, 2016

Kummerow, C. and W. Berg, A Fundamental Climate Data Record SSMI and SSMIS Science Data Stewardship, 2010 Workshop on Climate Data Records from Satellites, Silver Spring, MD, March 22-24, 2010. http://www.orbit.nesdis.noaa.gov/star/documents/meetings/CDR2010/talks/DayOne/Kummerow_C.pdf

Labroue, S., P. Gaspar, J. Dorandeu, O.Z. Zanife, F. Mertz, P. Vincent, and D. Choquet. 2004. Nonparametric estimates of the sea state bias for the Jason-1 radar altimeter. *Mar. Geod.* 27:453-481.

Lemoine, F.G., N.P. Zelensky, D.S. Chinn, D.E. Pavlis, D.D. Rowlands, B.D. Beckley, S.B. Luthcke, P. Willis, M. Ziebart, A. Sibthorpe, J. Boy, V. Luceri, Towards development of a consistent orbit series for TOPEX, Jason-1, and Jason-2, Adv. Space Research, 46 (2010) 1513-1540, doi: 10.1016/j.asr.2010.05.007

Lemoine, F.G., N.P. Zelensky, D.S. Chinn, B.D. Beckley, D.D. Rowlands, D.E. Pavlis (2015) A new time series of orbits (std1504) for TOPEX/Poseidon. Jason-1, and Jason-2 (OSTM), Ocean Surface Topography Science Team Meeting, Reston, VA. http://meetings.aviso.altimetry.fr/?id=95&nocache=1&tx_ausyclsseminar_pi2%5bobjAbstract%5d=1716&nocache=1&useCacheHash=1&cHash=1

Leuliette, E.W., and R. Scharroo, Integrating Jason-2 into a Multiple-Altimeter Climate Data Record, *Marine Geodesy*, 33(S1): 504-517, 2010, Supplemental Issue on OSTM/Jason-2 calibration/validation, Vol. 1, DOI: 10.1080/01490419.2010.487795.

Masters, D., R. S. Nerem, C. Choe, E. Leuliette, B. Beckley, N. White, M. Ablain (2012), "Comparison of global mean sea level time series from TOPEX/Poseidon, Jason-1, and Jason-2," *Marine Geodesy*, **35**, 20–41.

Mayer-Guerr, T. The combined satellite gravity field model goco05s. In EGU general assembly conference abstracts, volume 17, 2015.

Mitchum, G.T. 2000. An improved calibration of satellite altimetric heights using tide gauge sea levels with adjustment for land motion. *Marine Geodesy*, 23, 145-166.

Misra, S. and S. Brown, Application of a Mixed-Pixel Algorithm to TOPEX for Coastal Wet Tropospheric Delay Retrieval, 2011 Coastal Altimetry Workshop poster presentation.

Moreaux, G Willis P, Frank Lemoine F, Zelensky N, Couhert A, Hanane HAL, Ferrage P (2016), DPOD2014: a new DORIS extension of ITRF2014 for Precise Orbit Determination, 2016 AGU poster, http://ids-doris.org/documents/report/meetings/AGU2016_IDS_CC-DPOD2014-Moreaux.pdf

Nerem, R.S., D.P. Chambers, C. Choe, G.T. Mitchum, Estimating Mean Sea Level Change from the TOPEX and Jason Altimeter Missions, *Marine Geodesy*, 33(S1): 435-446, 2010, Supplemental Issue on OSTM/Jason-2 calibration/validation, Vol. 1, DOI: 10.1080/01490419.2010.491031.

Nerem, R. S., B.D. Beckley, J. T. Fasullo, B.D. Hamlington, D. Masters, and G. T. Mitchum, 2018. "Climate-change–driven accelerated sea-level rise detected in the altimeter era." *Proceedings of the National Academy of Sciences*, 201717312 [10.1073/pnas.1717312115]

OSTM/Jason-2 products handbook, Issue 1 rev 8, December 1, 2011. SALP-MU-M-OP-15815-CN(CNES), EUM/OPS-JAS/MAN/08/0041 (EUMETSAT), OSTM-29-1237 (JPL), Polar Series/OSTM J400 (NOAA/NESDIS).

Palanisamy, H., Meyssignac, B., Cazenave, A., Delcroix, T., 2015. Is antropogenic fingerprint of sea level already detectable in the Pacific Ocean? Environ. Res. Lett. 10 (8). http://dx.doi.org/10.1088/1748-9326/10/8/08402.

Peltier, W. R., 2009. Closure of the budget of global sea level rise over the GRACE era: The importance and magnitude of the required corrections for global glacial isostatic adjustment, Quat. Sci. Rev. 17–18:1658–1674, doi:10.1016/j.quascirev.2009.04.004.

Picot, N., K. Case, S. Desai, and P. Vincent. 2008. *AVISO and PODAAC User Handbook. IGDR and GDR Jason Products, Edition 4.0*. SMM-MU-M5-OP-13184-CN (**AVISO**), JPL D-21352 (**PODAAC**).

Picot, N., et al., 2016, Jason-3 Products Handbook, Issue 1, revision 2, February 12, 2016, CNES : SALP-MU-M-OP-16118-CN

Ponte, R. M. and R. D. Ray, "Atmospheric pressure corrections in geodesy and oceanography: a strategy for handling air tides," Geophysical Research Letters, 29(24), 2153, 2002.

Ray, R.D. 1999. A global ocean tide model from TOPEX/Poseidon altimetry: GOT99.2, NASA TM-1999-209478, NASA Goddard Space Flight Center, September 1999 (Update).

Ray, R.D., B.D. Beckley, F.G. Lemoine. Vertical crustal motion derived from satellite altimetry and tide gauges, and comparisons with DORIS measurements. Adv. Space Research, 45 (2010) 1510-1522, doi: 10.1016/j.asr.2010.02.020

Ray, R. D. and S.Y. Erofeeva (2014), Long-period tidal variations in the length of day, Journal of Geophysical Research: Solid Earth, 119, 1498-1509, doi:10.1002/2013JB010830.

Ray, R. D. and E. Zaron (2016), "M2 internal tides and their observed wavenumber spectra from satellite altimetry," J. Phys. Oceanogr., 46(1), 3-22. doi:10.1175/JPO-D-15-0065.1

Rudenko S, Dettmering D, Esselborn S, Schoene T, Foerste C, Lemoine J-M, Ablain M, Alexandre D, Neumayer K-H (2014) Influence of time variable geopotential models on precise orbits of altimetry satellites, global and regional mean sea level trends. Advances in Space Research, doi: 10.1016/j.asr.2014.03.010

Santamaría-Gómez, A., M. Gravelle, X. Collilieux, M. Guichard, B. Martín Míguez, P. Tiphaneau, and G. Wöppelmann (2012), Mitigating the effects of vertical land motion in tide gauge records using state-of-the-art GPS velocity field, Global Planet. Change, 98-99, 6–17.

Stammer, D., R.D. Ray, O.B. Andersen, et al., Accuracy assessment of global barotropic ocean tide models, Reviews of Geophysics, 2014.

TOPEX Ground System Science Algorithm Specification, JPL D-7075, Rev. A, Change 1; April 25, 1991.

Tran, N., Phillips, E. Bronner, and N. Picot, Impact of GDR_D standards on SSB corrections, Ocean Surface Topography Science Working Team Meeting, Venice, Italy, 2012. http://www.aviso.oceanobs.com/fileadmin/documents/OSTST/2012/oral/02_friday_28/01_instr_processing_I/01_IP1_Tran.pdf

Tran, N., S. Labroue, S. Phillips, E. Bronner, and N. Picot, Overview and Update of the Sea State Bias Corrections for the Jason-2, Jason-1, and TOPEX Missions. *Mar. Geod.* 33(S1): 348-362, 2010. DOI: 10.1080/01490419.2010.487788

Wöppelmann, G., C. Letetrel, A. Santamaria, M.-N. Bouin, X. Collilieux, Z. Altamimi, S.D.P. Williams, B. Martin Miguez, 2009. Rates of sea-level change over the past century in a geocentric reference frame. Geophys. Res. Lett. 36, L12607, 2009.

Zelensky, N.P., F.G. Lemoine, M. Ziebart, A. Sibthorpe, P. Willis, B.D. Beckley, S.M. Klosko, D.S. Chinn, D.D. Rowlands, S.B. Luthcke, D.E. Pavlis, V. Luceri (2010), DORIS/SLR POD modeling improvements for Jason-1 and Jason-2, Adv. Space Research, 46(12), 1541-1558, 2010. doi: 10.1016/j.asr.2010.05.008

Zelensky, N.P., F. G. Lemoine, B. Beckley, D. S. Chinn, S. Melachroinos, S. B. Luthcke G. Mitchum, O. Bordyugov, Improved Modelling of Time-Variable Gravity for Altimeter Satellite POD (2012), POD Splinter poster 2012 OSTST, Venice Italy.

Zelensky, N.P., F.G. Lemoine, M. Ziebart, A. Sibthorpe, P. Willis, B.D. Beckley, S.M. Klosko, D.S. Chinn, D.D. Rowlands, S.B. Luthcke, D.E. Pavlis, V. Luceri (2010), DORIS/SLR POD modeling improvements for Jason-1 and Jason-2, Adv. Space Research, 46(12), 1541-1558, 2010. doi: 10.1016/j.asr.2010.05.008

Zelensky, N.P., F.G. Lemoine, B.D. Beckley, D.S. Chinn, D.E. Pavlis, Impact of ITRS 2014 Realizations on Altimeter Satellite Precise Orbit Determination, *Advances in Space Research,* 10.1016/j.asr.2017.07.044.

Appendix I: Quality Flag Bit Distributions

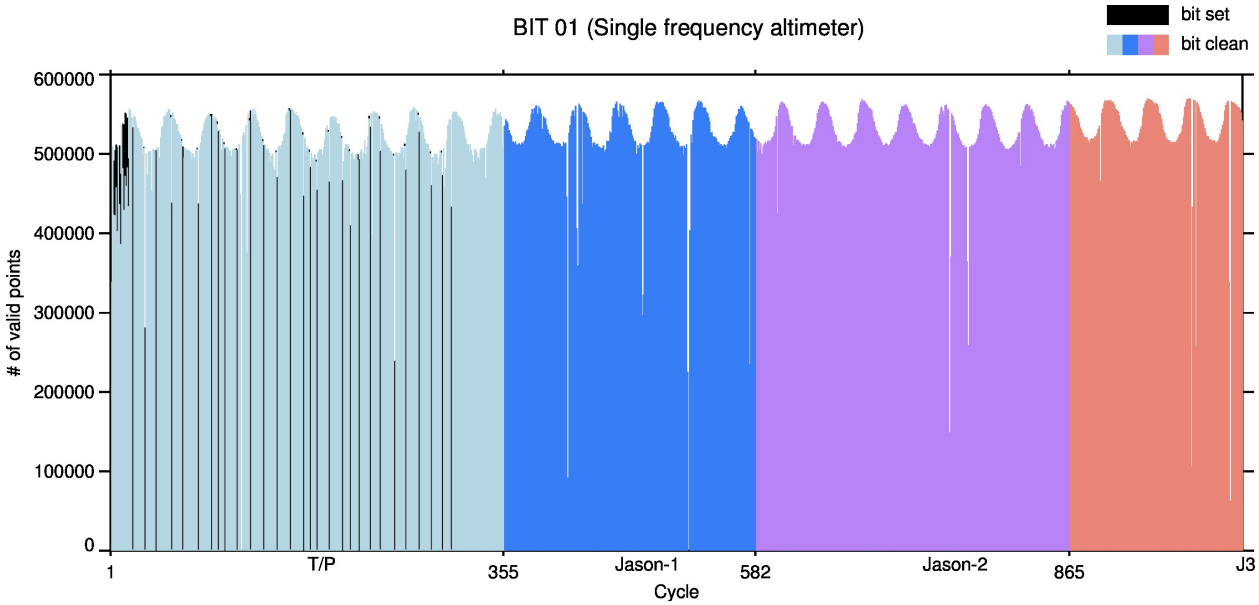

Figure A-1: Quality flag word Bit #1 when set to 1 indicates Poseidon-1 (single frequency) altimeter observations (see also Figure 17).

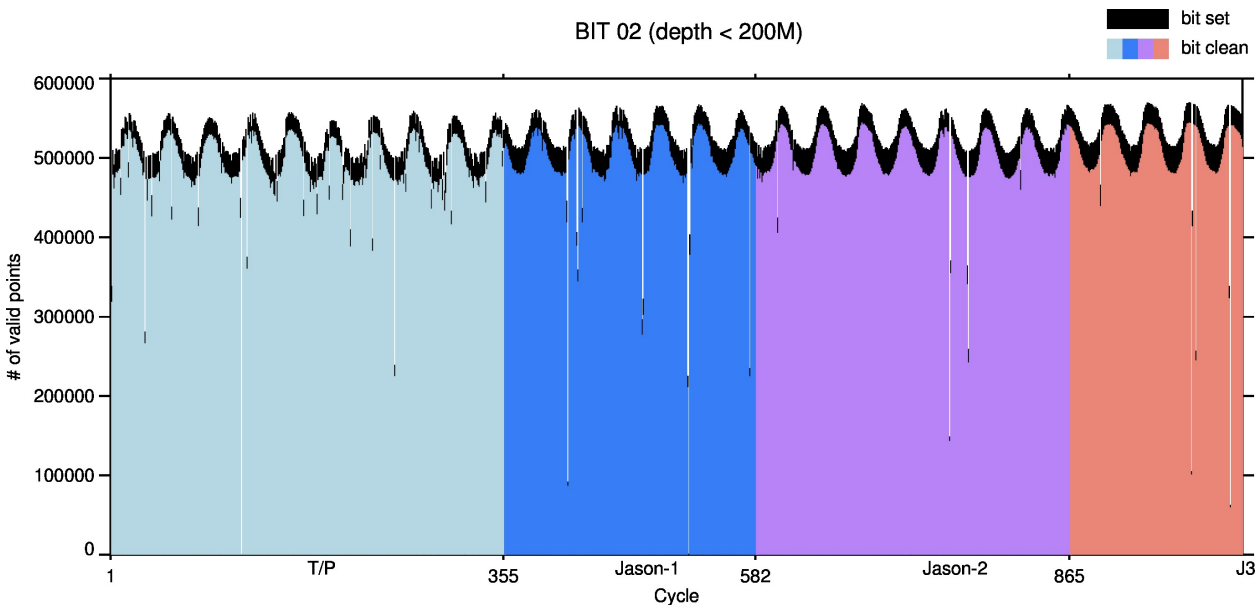

Figure A-2: Quality flag word Bit #2 when set to 1 indicates locations where ocean depth < 200 m.

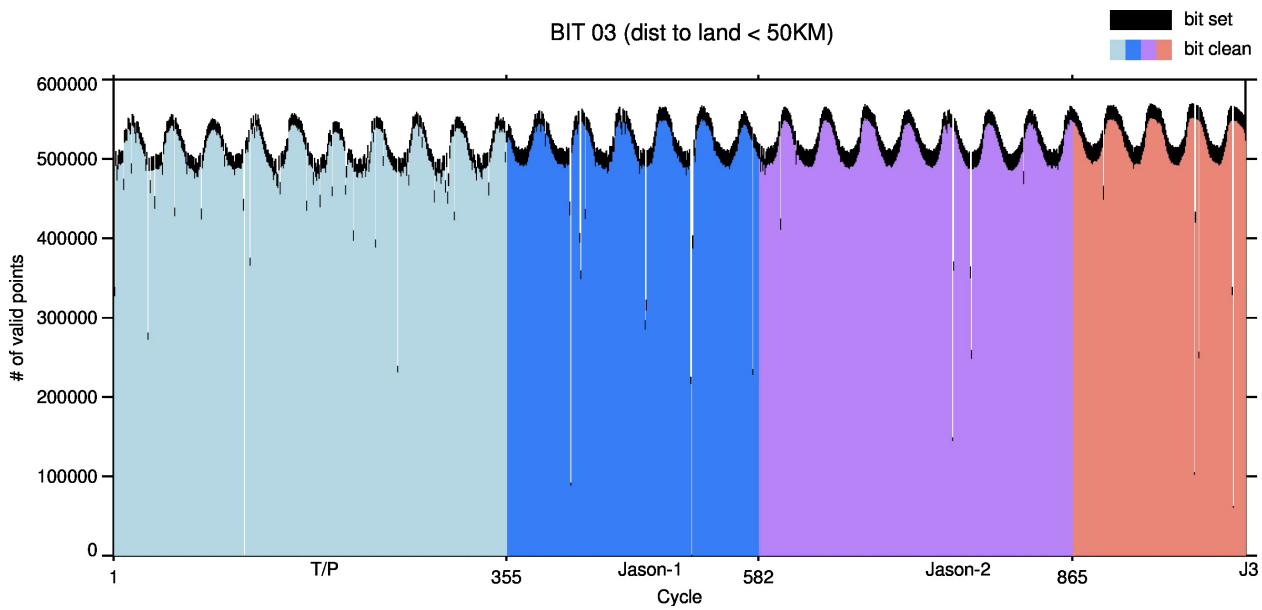

Figure A-3: Quality flag word bit #3 when set to 1 indicates locations within 50 km to coastline.

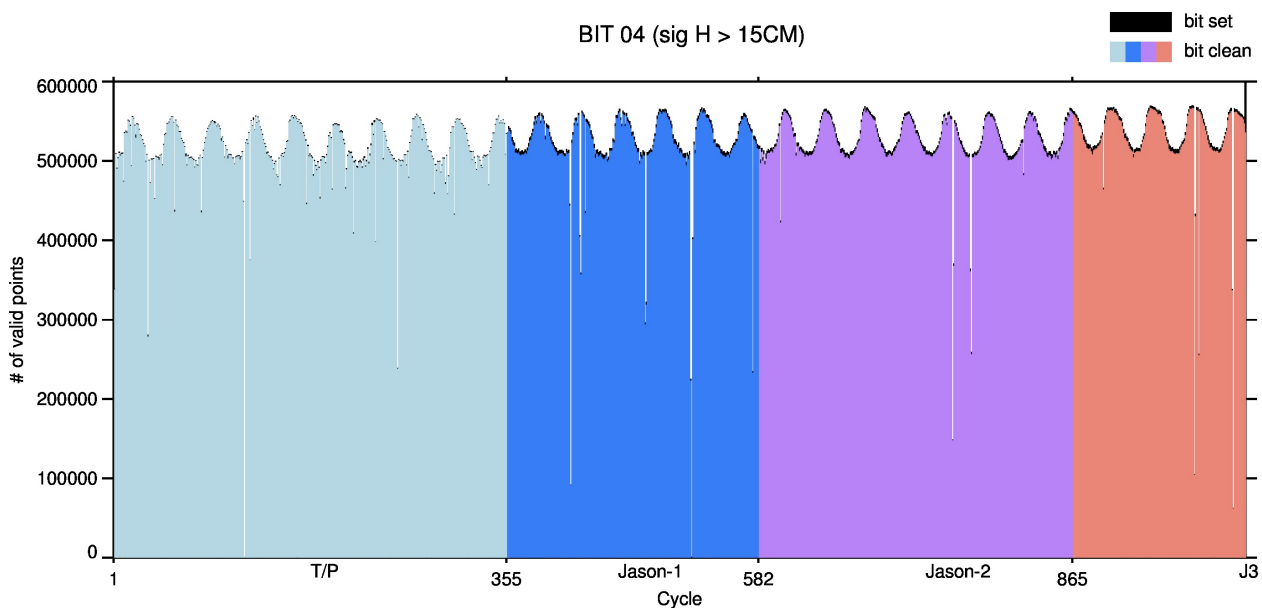

Figure A-4: Quality flag word bit #4 when set to 1 identifies 1Hz SSH measurements with standard deviation of high rate SSH residuals with respect to 1Hz "average" is greater than 15 cm (20 cm for Poseidon-1).

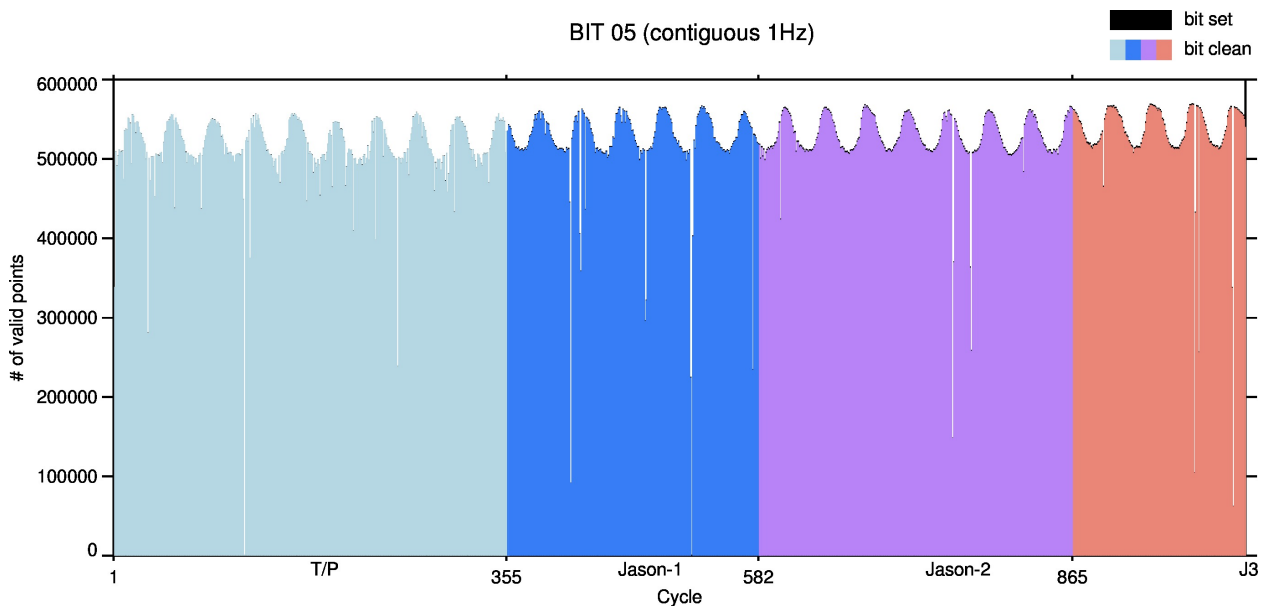

Figure A-5: Quality flag word bit #5 when set to 1 identifies 1Hz geo-referenced SSH values not derived from a nominal contiguous pair of high rate SSH measurements.

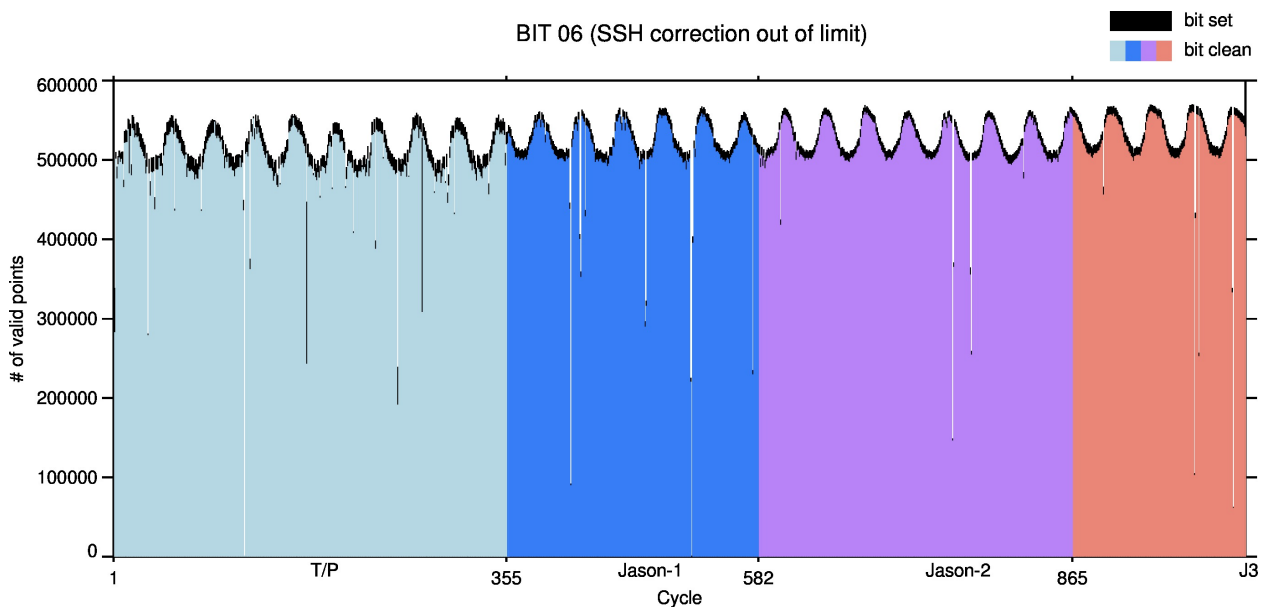

Figure A-6: Quality flag word bit #6 when set to 1 identifies valid (not equal to 32767) 1Hz geo-referenced SSH with one or more range or geophysical corrections outside nominal limits (see table 2).

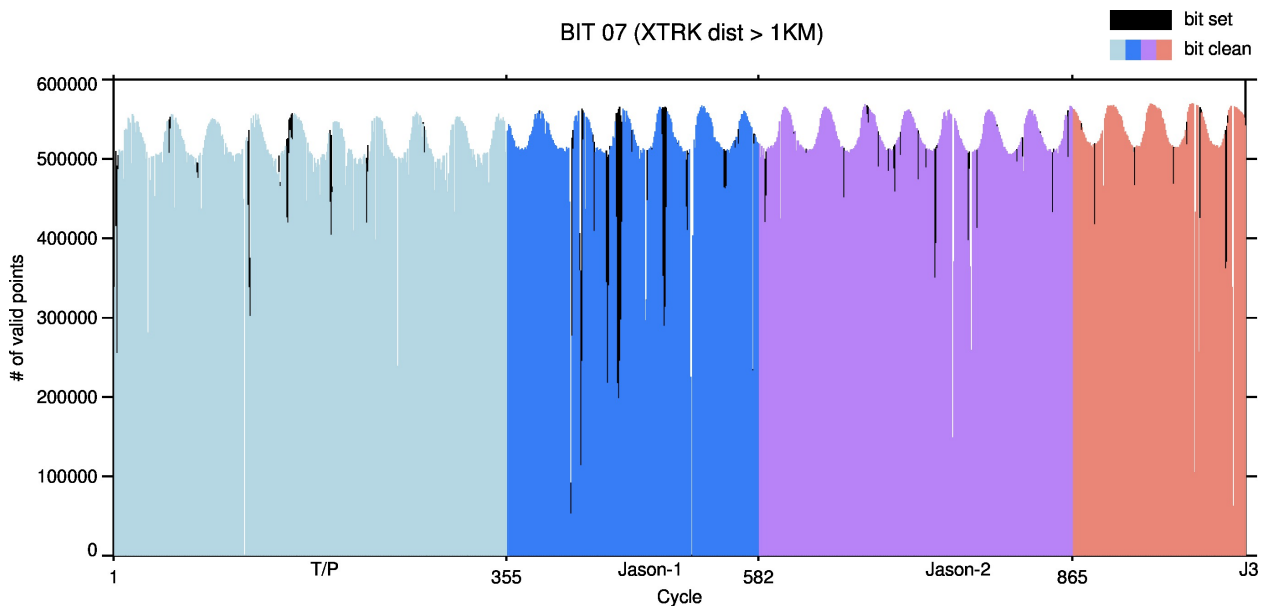

Figure A-7: Quality flag word bit #7 when set to 1 identifies locations with a cross-track distance > 1 km with respect to reference orbit.

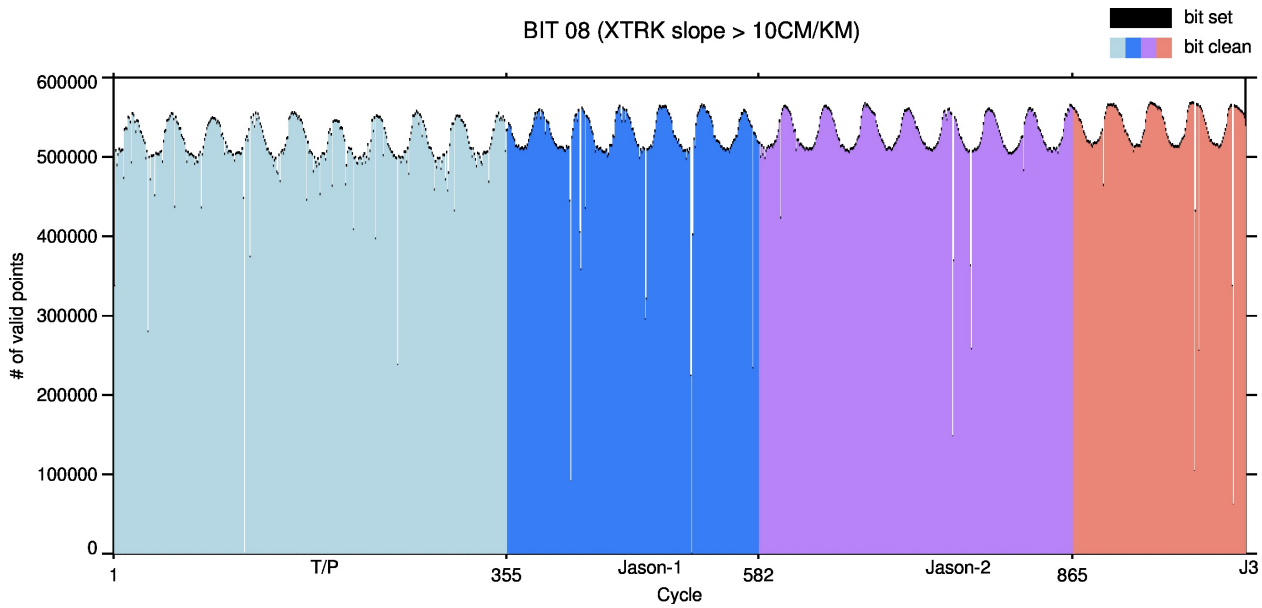

Figure A-8: Quality flag word bit #8 when set to 1 identifies locations with cross track geoid gradients exceeding 10 cm/km.

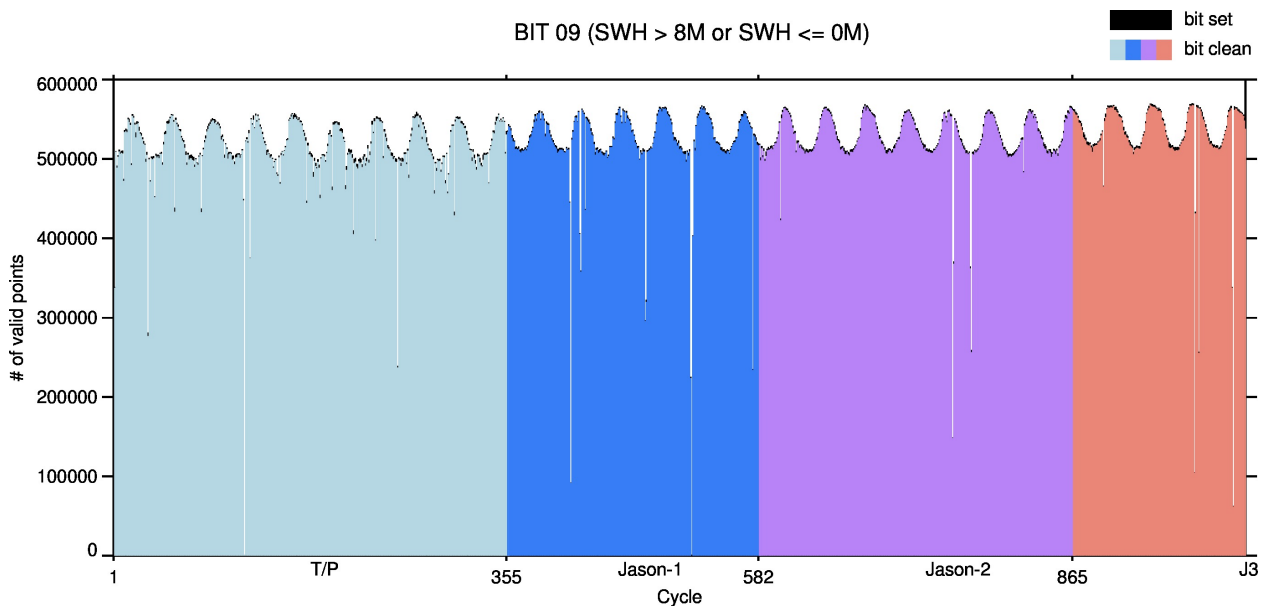

Figure A-9: Quality flag word bit #9 when set to 1 indicates SSH measurements at high sea states with SWH_Ku greater than 8.0 m, less than or equal to 0m.

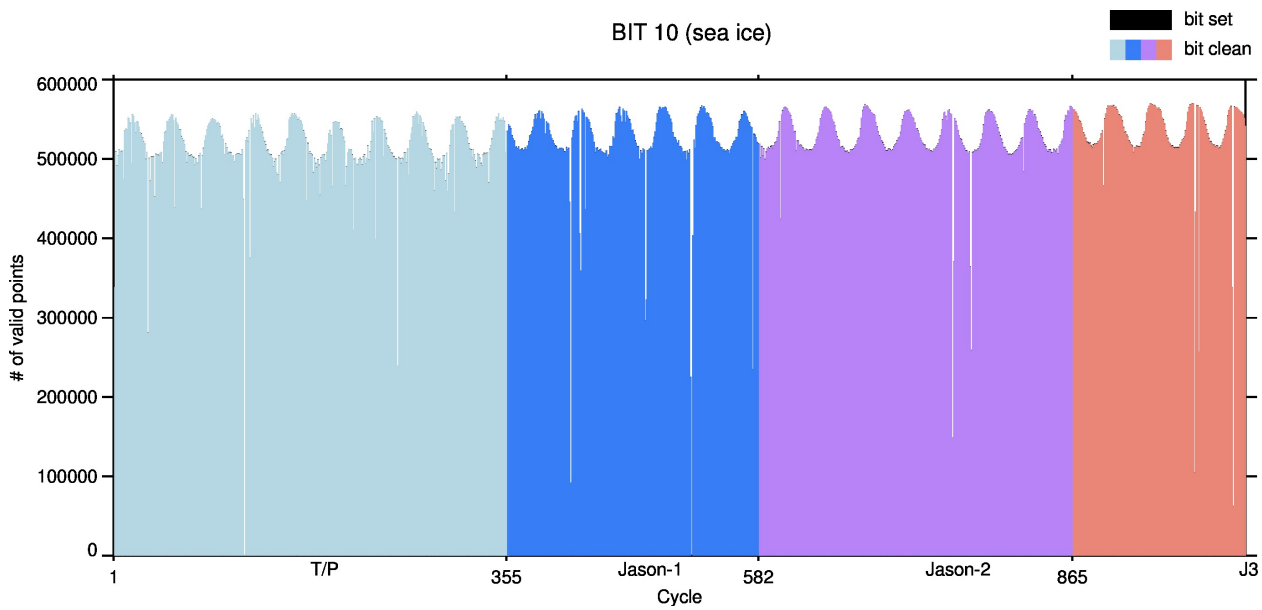

Figure A-10: Quality flag word bit #10 when set to 1 indicates observations with possible contamination of SSH estimate from presence of sea ice.

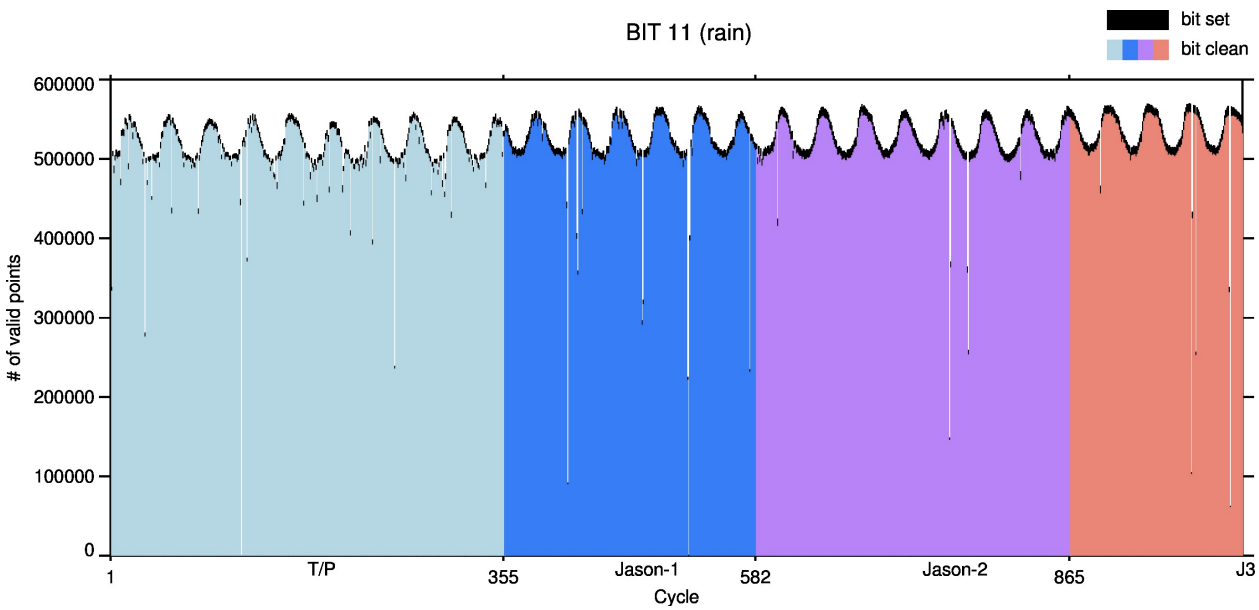

Figure A-11: Quality flag word bit 11 when set to 1 indicates observations with possible contamination of SSH estimate due to presence of rain.

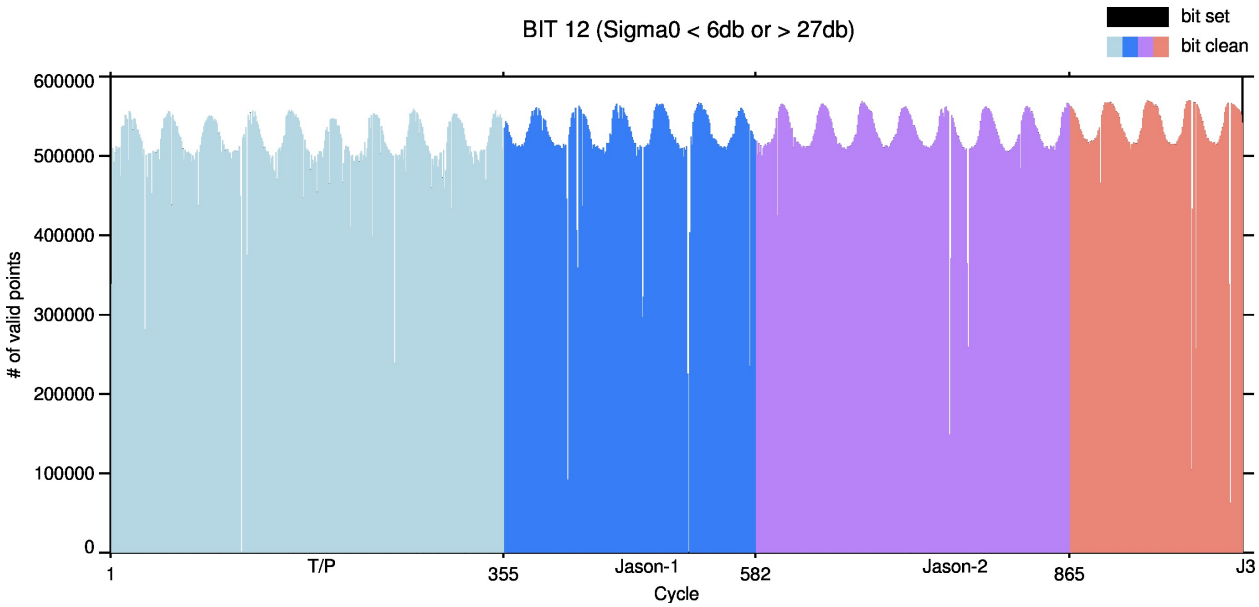

Figure A-12: Quality flag word bit #12 when set to 1 identifies observations with backscatter coefficients outside nominal range indicating high wind conditions or possible land/ice contamination.

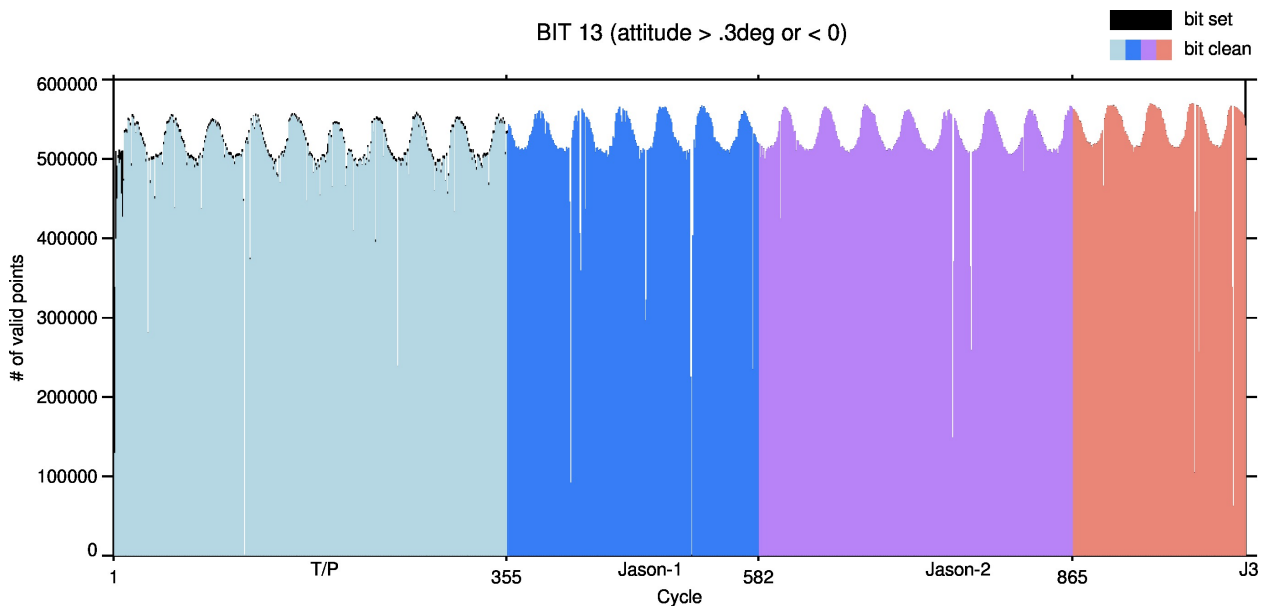

Figure A-13: Quality flag word bit #13 when set to 1 identifies observations when the attitude_waveform is outside nominal range limits.

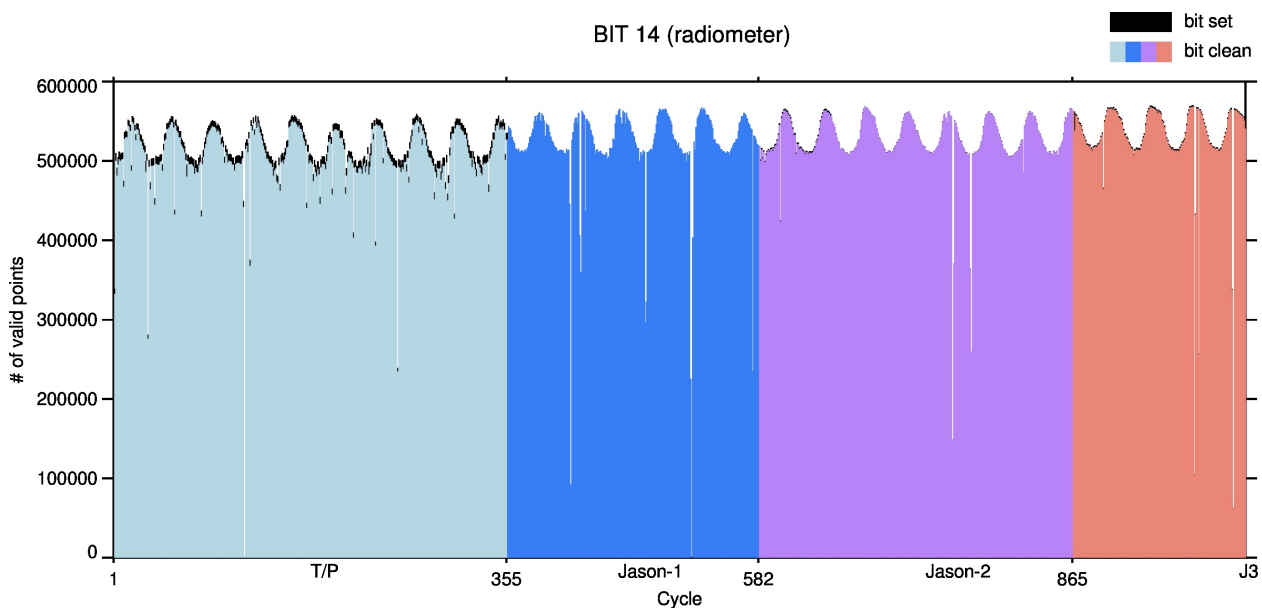

Figure A-14: Quality flag word bit #14 when set to 1 identifies observations where the radiometer measurement is believed to be suspect.

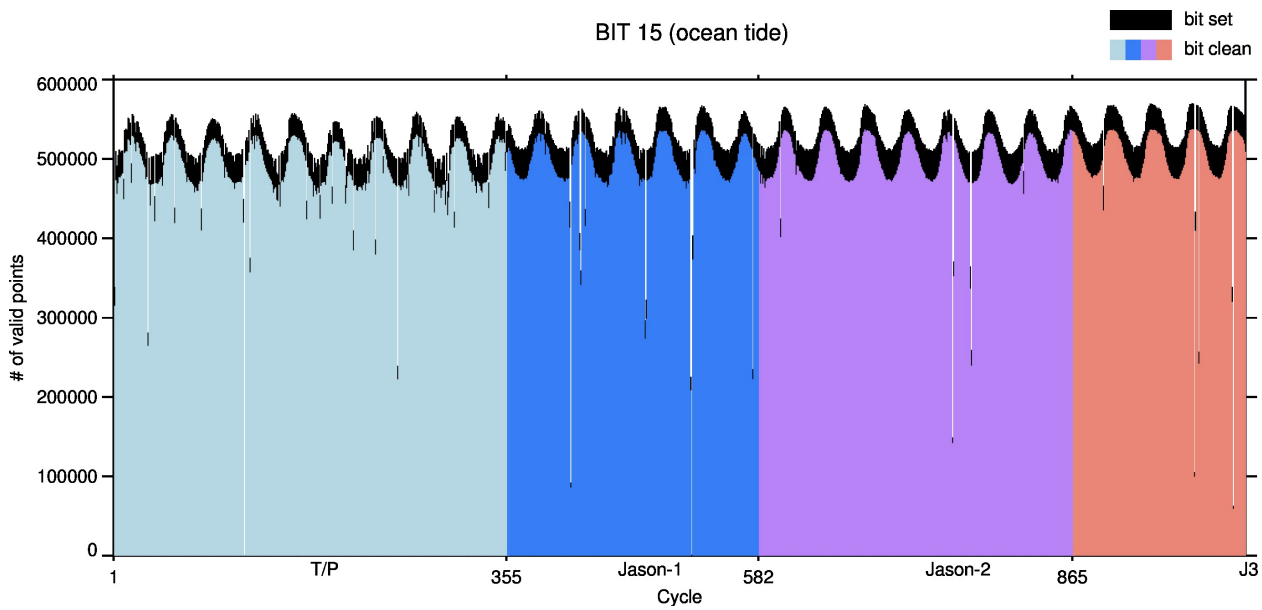

Figure A-15: Quality flag word bit #15 when set to 1 identifies coastal locations where the mean GOT4.8/FES04 ocean tide correction differs by more than 2.0 cm.

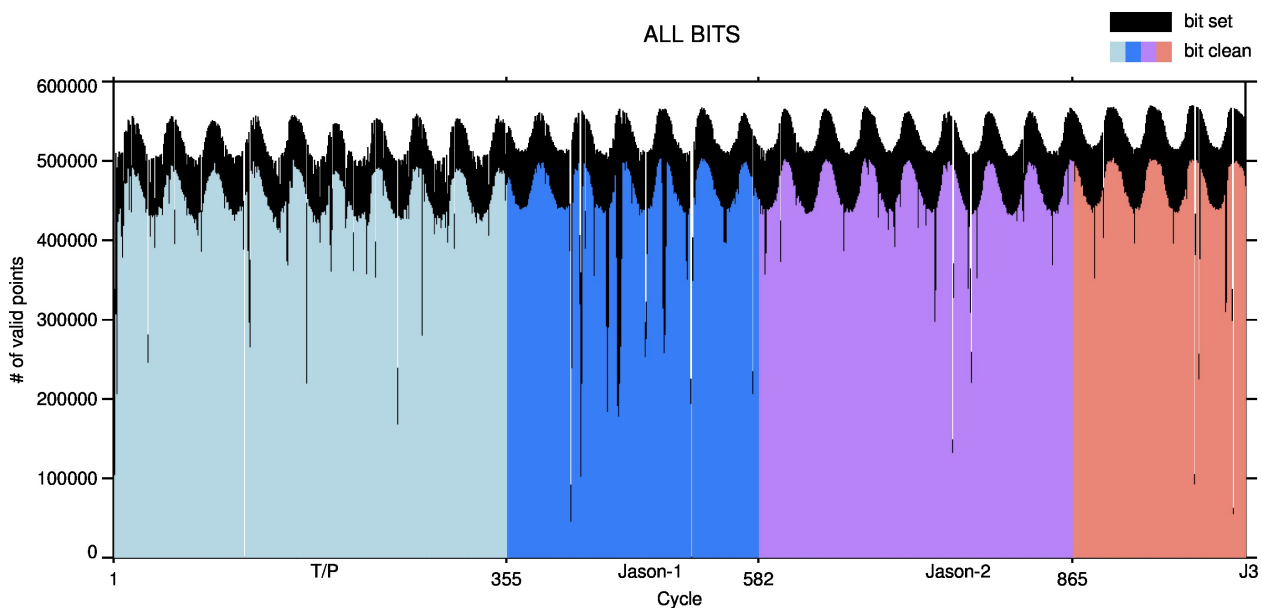

Figure A-16: An edit strategy that requires all bits set to 0 (except bit #1 to retain Poseidon-1 data) will result in ~ 10 % data loss.

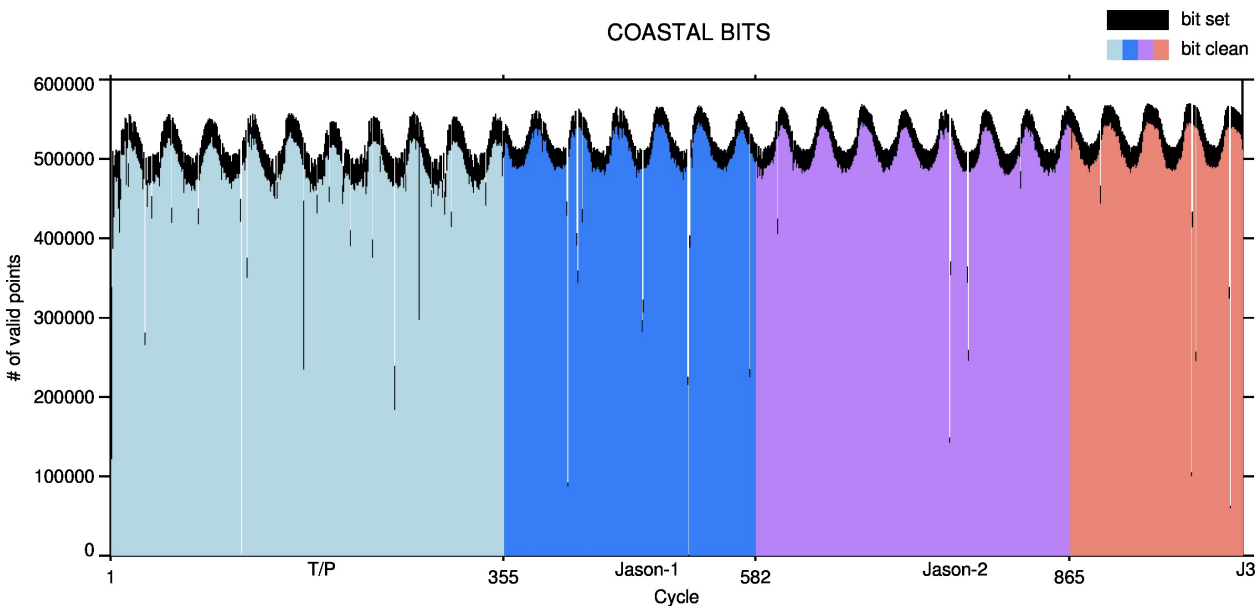

Figure A-17: Edit strategy as above except coastal observations are retained (bits 2,3, and 15) and both bits 7&8 in combination must be set, resulting in ~ 5 % data loss.

Appendix II: Sea State Bias Specifications

Jason-2&3: ssb_col_J2_Ku_mle4_1_36_v2012ostst.rs (Tran et al., 2012.)

Jason-1: ssb_col_J1_1_111_v2012ostst.rs (Tran et al., 2010)

TOPEX Side A: ssb_col_TPmgdr_021_131_v2009.rs (Tran et al., 2010)

TOPEX Side B: ssb_col_TPmgdr_240_350_v2009.rs (Tran et al., 2010)